De Rosa, E.; Latorre, M.; Montáns, FJ. (2017). Capturing anisotropic constitutive models with WYPiWYG hyperelasticity; and on consistency with the infinitesimal theory at all deformation levels. International Journal of Non-Linear Mechanics. 96:75-92. https://doi.org/10.1016/j.ijnonlinmec.2017.08.005

Capturing anisotropic constitutive models with WYPiWYG hyperelasticity, and on consistency with the infinitesimal theory at all deformation levels

Erica De Rosa[a], Marcos Latorre[b], Francisco J. Montáns[b,*]

[a] *Department of Industrial Engineering, Aerospace Division, University of Naples Federico II, Naples, Italy*
[b] *Escuela Técnica Superior de Ingeniería Aeronáutica y del Espacio, Universidad Politécnica de Madrid, Madrid, Spain*

Abstract

The elastic nonlinear behavior of fibre-reinforced materials and soft biological tissues is analysed using anisotropic hyperelastic models. Frequently, these models are not compatible with the corresponding infinitesimal theory, but some of them may be modified to accommodate that theory in the limit. WYPiWYG hyperelasticity is compatible with the infinitesimal theory at all deformation levels and capable of capturing exactly a complete set of experimental data, which reproduces all deformation modes at every strain level, under homogeneous deformations. In this work we study the relevance of recovering the infinitesimal theory at every deformed configuration and also the performance of the WYPiWYG method in predicting the behavior of anisotropic materials at large strains under nonhomogeneous deformations.

Keywords: Hyperelasticity, anisotropy, soft materials, transverse isotropy, large strains, biological tissues.

1. Introduction

The elastic behavior of fibre-reinforced materials and preconditioned soft tissues at large strains is modelled by anisotropic hyperelasticity [1], [2]. Anisotropic models usually consist of a stored energy of the matrix and a stored energy of the fibres. Following an affine deformations approach, these energies are assumed additive in

*Corresponding author
Email addresses: eri.derosa@studenti.unina.it (Erica De Rosa), m.latorre.ferrus@upm.es (Marcos Latorre), fco.montans@upm.es (Francisco J. Montáns)

the continuum. Even though physically motivated invariant sets are available [3], [4], [5], [6], the stored energies are usually formulated in terms of the Rivlin-Spencer invariants of the Cauchy-Green metric tensor [7], which have an elusive interpretation [8]. As explained by Murphy and co-workers [9], [10], [11], many of these models, as initially proposed, do not recover the infinitesimal theory from which they are motivated. Moreover, some models neglect the influence of some Rivlin-Spencer invariants resulting in an incomplete set to represent the different deformation modes at all deformation levels. Despite the common approach of neglecting some invariants, the necessity of using a complete set of invariants for the corresponding anisotropic case has been repeatedly reported [12], [13], [14], [15]. In summary, a model that recovers the infinitesimal theory should be able to represent all the *independent* deformation modes present in the infinitesimal limit without implicitly imposed couplings between them [10], unless those couplings have been experimentally verified. This is obviously a desirable feature to avoid nonphysical behavior [16], [17]; but it is also important in preserving the engineering intuition inherited from the infinitesimal theory, for example to be able to complete missing experimental data and to take advantage of known analytical solutions in the literature for some specific problems. To this end, we find important the use of physically motivated independent invariants as, for example, those presented in [3], [4], [5], [6] or the logarithmic ones we use below. An intuitive interpretation of the invariants employed in the formulations allows for understanding issues as their redundancy or independency, see Shariff et al [18], [19]. Furthermore, the physiological range, in which soft biological tissues work, is not unloaded. Hence, it is not only important to preserve the infinitesimal theory in the infinitesimal limit, *but also at all deformation levels*, because in fact, every incremental deformation may be considered an infinitesimal deformation over an updated reference configuration [20]. This means that all the independent deformation modes of the infinitesimal theory should remain independent (not implicitly coupled) at all deformation levels, unless experimental evidence supports a particular coupling assumption. This way, for example, the material parameters may be fitted using either the loaded or the unloaded configuration, which is a problem found in soft tissues when obtaining the material parameters of classical models [21]. In practice, for the transversely isotropic incompressible materials that we will consider in this paper, just as demonstrative examples, the recovery of the infinitesimal theory in the infinitesimal limit (i.e. reference configuration), means that three independent modes, and hence at least three material parameters (and their corresponding invariants), are needed [11]. However, when imposing infinitesimal *incremental* deformations at any strain level (any arbitrary configuration), the recovery of the independent deformation modes requires deformation-dependent material parameters which should be

determined from at least five independent experimental curves.

What-You-Prescribe-is-What-You-Get (WYPiWYG) hyperelasticity is a novel, purely numerical approach to obtain the stored energy of a hyperelastic material without imposing the form of the energy terms. The approach is based on the Sussman-Bathe idea [22] of employing local interpolations instead of global functions and the use of logarithmic invariants. We note that similar local interpolations to determine the stored energy function had been previously used also by Shariff [23], and that the use of logarithmic strains for hyperelasticity is traditional in computational plasticity [24], [25], [26], [27]. These types of invariants have also been extensively used in modelling soft materials by Criscione et al [5], [6].

The WYPiWYG method resembles the (local) finite element method in determining the stored energy through local interpolations, whereas the usual approach resembles the Rayleigh method in using global, assumed, analytical functions. The WYPiWYG method does not use material parameters nor optimization algorithms because it *solves* numerically the differential equations of the tests to obtain the stored energy, instead of *fitting* a proposed energy function. Hence, the method is specially suitable for addressing patient-specific modelling of soft biological tissues. There are WYPiWYG "models" for incompressible, transverse isotropic materials [28], for orthotropic materials [29] and for compressible materials [30]. A general procedure for determining the most general stored energies without inversion formula is given in Ref. [31]. As shown below, the theory is compatible with the infinitesimal theory *at all deformation levels* by construction, and captures to machine precision as many experimental curves as independent deformation modes. In this work we use the uncoupled WYPiWYG formulation to capture both homogeneous and nonhomogeneous deformations by two well-known models originally analyzed by Murphy in Ref. [9]: the standard reinforcing model and the Humphrey-Yin model. Uncoupled formulations have been also used by Shariff [32]. We discuss in detail the aspects of recovering the infinitesimal theory in the limit and at any deformed configuration, and we show that the WYPiWYG formulation is capable also of predicting the overall behavior of those models under large strain nonhomogeneous deformations, even relevant aspects of the models as for example the strain localization prediction of the standard reinforcing model; see [33] and references therein.

2. Motivation of WYPiWYG hyperelasticity: from infinitesimal strains to large strains

In this section we motivate the usual decompositions employed in WYPiWYG hyperelasticity from a parallel "bi-modular" infinitesimal framework which allows for

the possibility of different behavior in tension and compression. In the Appendix, an analysis of the Poynting effect in shear tests is given.

2.1. Infinitesimal theory for isotropic materials with different behavior in tension and compression

Assume the following infinitesimal strain energy decomposition in Valanis-Landel form

$$\Psi(\boldsymbol{\varepsilon}) = \mathcal{U}(\varepsilon_v) + \omega\left(\varepsilon_1^d\right) + \omega\left(\varepsilon_2^d\right) + \omega\left(\varepsilon_3^d\right) \tag{1}$$

where $\boldsymbol{\varepsilon}$ are the infinitesimal strains, $\varepsilon_v = tr(\boldsymbol{\varepsilon})$ is the volumetric strain and ε_i^d are the principal deviatoric strains. The functions $\mathcal{U}(\varepsilon_v)$ and $\omega\left(\varepsilon^d\right)$ are, respectively, the volumetric and the Valanis-Landel terms. These functions *need not be quadratic in the infinitesimal framework*, resulting in such cases in "material nonlinear only" (MNO) models, which are well known in the finite elements context; see [43]. For example, exponential hyperelastic functions are used within the infinitesimal strain context in soils [44]. We note that the decomposition Eq. (1) *is exact in the infinitesimal framework*, and can be specialized to the "bilinear" model (or "bi-quadratic" stored energy function)

$$\Psi(\boldsymbol{\varepsilon}) = \tfrac{1}{2}\kappa^{\#}\varepsilon_v^2 + \mu_1^*\left(\varepsilon_1^d\right)^2 + \mu_2^*\left(\varepsilon_2^d\right)^2 + \mu_3^*\left(\varepsilon_3^d\right)^2 \tag{2}$$

where $\kappa^{\#}$ and μ_i^* are material constants. The form in Eq. (2) may accommodate "bi-modular" materials, in which the constants take different values in tension and in compression, e.g.

$$\kappa^{\#} = \left\{ \begin{array}{l} \kappa^t \ \text{ if } \ \varepsilon_v \geq 0 \\ \kappa^c \ \text{ if } \varepsilon_v < 0 \end{array} \right\} \quad \text{and} \quad \mu_i^{\#} = \left\{ \begin{array}{l} \mu^t \ \text{ if } \ \varepsilon_i^d \geq 0 \\ \mu^c \ \text{ if } \varepsilon_i^d < 0 \end{array} \right\}, i = 1,2,3 \tag{3}$$

and, obviously, the fully linear theory is recovered if $\kappa \equiv \kappa^t = \kappa^c$ and $\mu \equiv \mu^t = \mu^c$. It is straightforward to relate the Young moduli Y^t, Y^c and the Poisson ratios ν^t, ν^c during tension/compression uniaxial tests to the previous moduli through

$$Y^t = \frac{(2\mu^t + \mu^c)\,9\kappa^t}{2\mu^t + \mu^c + 9\kappa^t}, \quad \nu^t = \frac{-4\mu^t - 2\mu^c + 9\kappa^t}{4\mu^t + 2\mu^c + 18\kappa^t} \tag{4}$$

$$Y^c = \frac{(2\mu^c + \mu^t)\,9\kappa^c}{2\mu^c + \mu^t + 9\kappa^c}, \quad \nu^c = \frac{-4\mu^c - 2\mu^t + 9\kappa^c}{4\mu^c + 2\mu^t + 18\kappa^c} \tag{5}$$

The stress tensor is also immediately obtained as

$$\boldsymbol{\sigma} = \frac{d\Psi\left(\boldsymbol{\varepsilon}\right)}{d\boldsymbol{\varepsilon}} = \frac{d\Psi\left(\varepsilon_v, \varepsilon_i^d\right)}{d\boldsymbol{\varepsilon}} = \kappa^{\#}\varepsilon_v \frac{d\varepsilon_v}{d\boldsymbol{\varepsilon}} + \sum_{i=1}^{3} 2\mu_i^* \varepsilon_i^d \frac{d\varepsilon_i^d}{d\boldsymbol{\varepsilon}^d} : \frac{d\boldsymbol{\varepsilon}^d}{d\boldsymbol{\varepsilon}} \tag{6}$$

$$= \kappa^{\#}\varepsilon_v \boldsymbol{I} + \sum_{i=1}^{3} \left(2\mu_i^* \varepsilon_i^d\right) \left(\boldsymbol{N}_i \otimes \boldsymbol{N}_i\right) : \mathbb{P} = \boldsymbol{\sigma}^v + \boldsymbol{\sigma}^{|d} : \mathbb{P} \tag{7}$$

where $\boldsymbol{N}_i$ are the principal stress/strain directions, $\mathbb{P} = \mathbb{I} - (1/3)\,\boldsymbol{I} \otimes \boldsymbol{I}$ is the deviatoric projector tensor, $\boldsymbol{\sigma}^v$ is the volumetric part of stresses and $\boldsymbol{\sigma}^d = \boldsymbol{\sigma}^{|d} : \mathbb{P}$ is the deviatoric counterpart. The operators "$\otimes$" and ":" are, respectively, the dyadic (outer) product and the double-index contraction product (i.e. the scalar product between second order tensors). The tensors $\boldsymbol{I}$ and $\mathbb{I}$ are, respectively, the second- and fourth-order (symmetric) identity tensors. The tangent is

$$\mathbb{C} = \frac{d^2\Psi\left(\boldsymbol{\varepsilon}\right)}{d\boldsymbol{\varepsilon} d\boldsymbol{\varepsilon}} = \kappa^{\#}\boldsymbol{I} \otimes \boldsymbol{I} + \mathbb{P} : \sum_{i=1}^{3} 2\mu_i^* \mathbb{N}_{iiii} : \mathbb{P} \tag{8}$$

$$+ \mathbb{P} : \sum_{i=1}^{3} \sum_{j \neq i} \frac{2\mu_j^* \varepsilon_j^d - 2\mu_i^* \varepsilon_i^d}{\varepsilon_j^d - \varepsilon_i^d} \frac{1}{2} \left(\mathbb{N}_{ijij} + \mathbb{N}_{ijji}\right) : \mathbb{P}$$

where we defined the fourth-order tensor $\mathbb{N}_{ijkl} = \boldsymbol{N}_i \otimes \boldsymbol{N}_j \otimes \boldsymbol{N}_k \otimes \boldsymbol{N}_l$. In principal directions, the non-trivial 3×3 part of the matrix relating stresses to strains in principal directions is

$$\{\mathbb{C}\} = \begin{bmatrix} \kappa^{\#} & \kappa^{\#} & \kappa^{\#} \\ \kappa^{\#} & \kappa^{\#} & \kappa^{\#} \\ \kappa^{\#} & \kappa^{\#} & \kappa^{\#} \end{bmatrix} + \begin{bmatrix} \frac{2}{3} & -\frac{1}{3} & -\frac{1}{3} \\ -\frac{1}{3} & \frac{2}{3} & -\frac{1}{3} \\ -\frac{1}{3} & -\frac{1}{3} & \frac{2}{3} \end{bmatrix} \begin{bmatrix} 2\mu_1^* & 0 & 0 \\ 0 & 2\mu_2^* & 0 \\ 0 & 0 & 2\mu_3^* \end{bmatrix} \begin{bmatrix} \frac{2}{3} & -\frac{1}{3} & -\frac{1}{3} \\ -\frac{1}{3} & \frac{2}{3} & -\frac{1}{3} \\ -\frac{1}{3} & -\frac{1}{3} & \frac{2}{3} \end{bmatrix} \tag{9}$$

$$= \begin{bmatrix} \kappa^{\#} & \kappa^{\#} & \kappa^{\#} \\ \kappa^{\#} & \kappa^{\#} & \kappa^{\#} \\ \kappa^{\#} & \kappa^{\#} & \kappa^{\#} \end{bmatrix} + \frac{2}{9} \begin{bmatrix} 4\mu_1^* + \mu_2^* + \mu_3^* & \mu_3^* - 2\mu_2^* - 2\mu_1^* & \mu_2^* - 2\mu_1^* - 2\mu_3^* \\ \mu_3^* - 2\mu_2^* - 2\mu_1^* & \mu_1^* + 4\mu_2^* + \mu_3^* & \mu_1^* - 2\mu_2^* - 2\mu_3^* \\ \mu_2^* - 2\mu_1^* - 2\mu_3^* & \mu_1^* - 2\mu_2^* - 2\mu_3^* & \mu_1^* + \mu_2^* + 4\mu_3^* \end{bmatrix} \tag{10}$$

The relevance of this framework can be understood when it is compared to recent formulations for bi-modular materials [34], [35]: our formulation is motivated from hyperelasticity, has a very simple finite element implementation and has no restriction in the material constants —cf. Eq. (1) in [34]. Furthermore, the extension to

anisotropy and nonlinear behaviour is straightforward as seen below.

2.2. WYPiWYG isotropic formulation

In order to make explicit the reference configuration and the instant at which measures refer, we use a frequent notation in computational mechanics (see e.g. Ref. [43]). In this notation, left super- and sub-indices are employed to respectively emphasize the current and the reference configurations when applicable. For example ${}^{t}_{0}\boldsymbol{U}$ denotes the stretch tensor $\boldsymbol{U}$ from the reference configuration at time $\tau = 0$ to the current configuration at time $\tau = t$. In a similar manner, ${}^{t}\boldsymbol{\sigma}$ are the Cauchy stresses at time t, and $d_t\boldsymbol{\varepsilon}$ are the infinitesimal strains measured at configuration t. In a uniaxial problem $d_t\varepsilon = dl/l$, where $l = {}^{t}l$ is the current length. Note that $(d\varepsilon =)\ d_0\varepsilon = dl/{}^{0}l \neq dl/{}^{t}l = d_t\varepsilon = d^t_0E$, where ${}^{t}_{0}E = \ln({}^{t}l/{}^{0}l)$. An infinitesimal strain over the current configuration is given by $d_t\varepsilon \equiv d^t_0E$.

Logarithmic strains have some interesting properties. Assume that the principal directions of deformation are kept fixed. Then let ${}^{t+\Delta t}_{0}\boldsymbol{U} = {}^{t+\Delta t}_{t}\boldsymbol{U}\ {}^{t}_{0}\boldsymbol{U}$ be the stretch tensor at $t+\Delta t$ obtained from that at t, ${}^{t}_{0}\boldsymbol{U}$, and let ${}^{t+\Delta t}_{0}\boldsymbol{E} = \ln {}^{t+\Delta t}_{0}\boldsymbol{U}$ be the logarithmic strain tensor. We can write [37]

$$ {}^{t+\Delta t}_{0}\boldsymbol{E} = \ln\ {}^{t+\Delta t}_{0}\boldsymbol{U} = \ln\ {}^{t+\Delta t}_{t}\boldsymbol{U} + \ln\ {}^{t}_{0}\boldsymbol{U} = {}^{t+\Delta t}_{t}\boldsymbol{E} + {}^{t}_{0}\boldsymbol{E} \tag{11} $$

In fact, the dilatational component is always additive, even if principal directions change, and is computed in the same form as the infinitesimal strains. If principal directions are not preserved during the real deformation path, because strains are a state function of the deformation (i.e. they depend on the final displacements, but not on how we arrived at those values), we can always think of a deformation path in which principal directions are kept fixed. Then, it can be shown that logarithmic strains are the addition of all infinitesimal strains, and that the rate of infinitesimal strains may be interpreted as a fictitious velocity gradient $\dot{\boldsymbol{\varepsilon}} = \dot{\boldsymbol{\Upsilon}}\boldsymbol{\Upsilon}^{-1}$, see [37]

$$ {}^{t}_{0}\boldsymbol{E} = \int_0^t d_\tau\boldsymbol{\varepsilon} = \int_0^t \dot{\boldsymbol{\varepsilon}}\,(\tau)\,d\tau = \int_0^t {}^{\tau}\dot{\boldsymbol{\Upsilon}}\ {}^{\tau}_{0}\boldsymbol{\Upsilon}^{-1} d\tau \tag{12} $$

with

$$ {}^{\tau}\dot{\boldsymbol{\Upsilon}} = \sum_{i=1}^{3} {}^{\tau}\dot{\lambda}_i \boldsymbol{N}_i \otimes \boldsymbol{N}_i \tag{13} $$

Then, using $\varepsilon_v = tr\,(\boldsymbol{\varepsilon})$, we can write

$$ {}^{t}_{0}\boldsymbol{E} = \frac{1}{3}\,{}^{t}_{0}E_v\boldsymbol{I} + \sum_{i=1}^{3}\,{}^{t}_{0}E^d_i\;\boldsymbol{M}_i = \left(\frac{1}{3}\int_0^t d_\tau\varepsilon_v\right)\boldsymbol{I} + \sum_{i=1}^{3}\left(\int_0^t d_\tau\varepsilon^d_i\right)\;\boldsymbol{M}_i \tag{14} $$

and we have *in the most general case*

$$ {}^{t}_{0}E_v = \ln\,{}^{t}_{0}J = \int_0^t d_\tau\varepsilon_v \tag{15} $$

and in the fictitious path with principal directions fixed

$$ {}^{t}_{0}E^d_i = \int_0^t d_\tau\varepsilon^d_i \tag{16} $$

Remarkably, in contrast to the shear terms of other strain measures, it can be shown that the shear terms of the logarithmic strains give a physically accurate representation of shear deformations when interpreted as area distortions [37] (which is an interpretation valid for both infinitesimal shear strains and logarithmic shear strains). Furthermore, as it is well-known, spatial logarithmic strains are obtained just from a rotation of the material ones. With all these properties, it should not be a surprise that the volumetric and deviatoric projections are performed exactly as in the infinitesimal case, regardless of considering referential, incremental or spatial configurations.

The interpretation of Equation (12) is that at any given instant τ, the successive incremental deformations have the structure of infinitesimal deformations. Furthermore, we can quantify the deformation process from the reference configuration to a state $\tau + d\tau$ following a succession of infinitesimal, rotationless *additive strains* i.e. ${}^{\tau+d\tau}_{\tau}\boldsymbol{E} = {}^{\tau+d\tau}_{\tau}\boldsymbol{\varepsilon} \equiv d_\tau\boldsymbol{\varepsilon}$. In this rotationless case with principal directions fixed, we can linearize the stress-strain relation as—$\boldsymbol{T}$ are the generalized Kirchhoff stresses, work-conjugate to the referential logarithmic strains [38], as we see below

$$ {}^{\tau+d\tau}\boldsymbol{T} = {}^{\tau}\boldsymbol{T} + {}_{\tau}\kappa^{\#}\;d_\tau\varepsilon_v\boldsymbol{I} + \sum_{i=1}^{3} 2\;{}_{\tau}\mu^*_i\;d_\tau\varepsilon^d_i\;\boldsymbol{M}_i : \mathbb{P} \tag{17} $$

and we can integrate this relation to give

$$ {}^{t}\boldsymbol{T} = \left(\int_0^t\;{}_{\tau}\kappa^{\#}\;d_\tau\varepsilon_v\right)\boldsymbol{I} + \sum_{i=1}^{3}\left(\int_0^t 2\;{}_{\tau}\mu^*_i\;d_\tau\varepsilon^d_i\right)\;\boldsymbol{M}^d_i \tag{18} $$

where we denoted $\boldsymbol{M}_i^d = \boldsymbol{M}_i : \mathbb{P}$. Define

$$\mathcal{U}'\left(E_v\left(t\right)\right) = \frac{d\mathcal{U}\left(E_v\left(t\right)\right)}{dE_v} := \int_0^t {}_\tau\kappa^{\#}\, d_\tau\varepsilon_v \equiv \int_0^t {}_\tau\kappa^{\#}\, d_\tau E_v \tag{19}$$

$$\omega'\left(E_i^d\left(t\right)\right) = \frac{d\omega\left(E_i^d\left(t\right)\right)}{dE_i^d} := \int_0^t 2\ {}_\tau\mu_i^*\, d_\tau\varepsilon_i^d \ = \int_0^t 2\ {}_\tau\mu_i^*\, d_\tau E_i^d \tag{20}$$

Then, allowing non-constant ${}_\tau\kappa^{\#}$ and ${}_\tau\mu_i^*$

$$\mathcal{U}''\left(E_v\right) = \left.\frac{d^2\mathcal{U}}{dE_v^2}\right|_\tau \equiv \left.\frac{d^2\mathcal{U}}{dE_v^2}\right|_{{}_\tau E_v} = {}_\tau\kappa^{\#} \equiv \kappa\left(E_v\right) \tag{21}$$

$$\omega''\left(E_i^d\right) = \left.\frac{d^2\omega}{dE_i^d dE_i^d}\right|_{{}_\tau E_i^d} = 2\ {}_\tau\mu_i^* \equiv 2\mu\left(E_i^d\right) \tag{22}$$

It is immediate to verify that the following (Valanis-Landel type) stored energy results in the stresses Eq. (18)—cf. Eq. (1)

$$\Psi\left(\boldsymbol{E}\right) = \mathcal{U}\left(E_v\right) + \omega\left(E_1^d\right) + \omega\left(E_2^d\right) + \omega\left(E_3^d\right) \tag{23}$$

Obviously, this stored energy is valid in a general, nonproportional, loading case, regardless of how it has been obtained (usually by means of experiments using proportional loading). The generalized Kirchhoff stresses (or the rotated Kirchhoff stresses in this isotropic case), work-conjugate to the referential logarithmic strains [38], are —cf. Eq. (7)

$$\boldsymbol{T} := \frac{d\Psi\left(\boldsymbol{E}\right)}{d\boldsymbol{E}} = \mathcal{U}'\left(E_v\right)\boldsymbol{I} + \sum_{i=1}^{3} \omega'\left(E_i^d\right)\boldsymbol{M}_i^d \tag{24}$$

and the tangent is —cf. Eq. (8)

$$\begin{aligned}\mathbb{C} = \frac{d^2\Psi\left(\boldsymbol{E}\right)}{d\boldsymbol{E}d\boldsymbol{E}} = \mathcal{U}''\left(E_v\right)\boldsymbol{I}\otimes\boldsymbol{I} + \mathbb{P} : \sum_{i=1}^{3} \omega''\left(E_i^d\right)\mathbb{N}_{iiii} : \mathbb{P} \\ + \mathbb{P} : \sum_{i=1}^{3}\sum_{j\neq i} \frac{T_j^d - T_i^d}{E_j^d - E_i^d}\frac{1}{2}\left(\mathbb{N}_{ijij} + \mathbb{N}_{ijji}\right) : \mathbb{P}\end{aligned} \tag{25}$$

This tangent may be systematically converted to any other work-conjugate stress-strain measures through proper mapping tensors [38].

2.3. An example of a computational procedure for WYPiWYG hyperelasticity

For simplicity consider an incompressible isotropic material following the previous Valanis-Landel form. The equilibrium equation of a tensile test is [22], [45]

$$\sigma(E) = \omega'(E) - \omega'\left(-\tfrac{1}{2}E\right) \tag{26}$$

where σ is the tensile stress and E is the longitudinal true strain. Assume that the experimental data consists of K pairs $\{E_k, \sigma_k\}$, $k = 1, ..., K$. The equilibrium Equation (26) cannot be solved in analytical form, but it can be easily solved numerically in many different ways. We show here a simple one using the inversion formula from Kearsley and Zapas. It can be shown that the solution of this equation at the experimental points is given by the Kaersley-Zapas formula which can be written [45] as

$$\omega'(E_k) = \sum_{n=0}^{\infty} \sigma\left(\left(-\frac{1}{2}\right)^n E_k\right) \tag{27}$$

where we have taken $\omega'(0) = 0$. Since it is usually assumed that $\sigma(0) = 0$, and $(-1/2)^n \to 0$ for $n \to \infty$, the series converge in a finite number of terms. This observation is important, because otherwise Eq. (27) would not be computationally useful. From a test we do not have a continuous curve $\sigma(E)$, but discrete pairs $\{E_k, \sigma_k\}$. However, it is straightforward to create a continuous function (for example a piecewise spline) $\sigma(E)$ from the available data. The function does not need to be analytical because we just need to evaluate it at points $(-1/2)^n E_k$ in the inversion formula Eq. (27). Once this function is created, it is used in the addends of the inversion formula Eq. (27) to obtain the values $\varpi_k \equiv \omega'(E_k)$. For each E_k value, the series terms $\sigma((-1/2)^n E_k)$, computed from evaluations of the previously computed continuous $\sigma(E)$ function, are successively added in a loop to the iteratively computed value of $\omega'(E_k)$, until the terms become smaller than a prescribed tolerance. Speed of convergence depends on the actual curve. In our experience, machine precision is reached typically in about 50 addends, but about 10 addends give usually indistinguishable solutions. Finally, with the discrete values ϖ_k, $k = 1, ..., K$, a continuous $\omega'(E)$ function is built. In this case we usually want $\omega''(E)$ to be smooth, so piecewise cubic splines (polynomials) are an excellent choice. Again, for computational procedures we do not need an analytical function, but just the possibility of evaluating $\omega'(E)$ (for stresses) and $\omega''(E)$ (for constitutive tangents) at any given value E. Needless to say that since the function $\omega'(E)$ contains the exact solution of the equilibrium equation at the experimental points $\{E_k, \sigma_k\}$, that experiment will be exactly reproduced in any numerical procedure. Furthermore, since the energy terms $\omega(E)$ are unique for materials following the Valanis-Landel decomposition,

any loading situation, proportional or nonproportional, will be captured to a high accuracy if enough experimental pairs are used in its determination [30].

2.4. Discussion about coupling terms

The uncoupled Equation (23) converges to the exact infinitesimal form Eq. (1), but many other large strain models do so as long as coupling terms between principal strains vanish in the infinitesimal regime. For moderately large strains typically found in soft tissues, say $\lambda_1 = 1.2$ (20%), we have $E_1 = 0.18$ and, if transverse strains are of the same order, $E_1 E_2 = 0.03$, which is a much smaller number. Then it is to be expected that coupling terms are small in usual loading situations, unless strains are very large in two directions simultaneously and coupling terms become relevant in the specific material at hand. It has been verified that these coupling terms are negligible in many materials for quite large strains, see for example [41].

3. Motivation of anisotropic WYPiWYG hyperelasticity in uncoupled form

In this section we extend the previous ideas for orthotropic and transversely isotropic materials.

3.1. Orthotropic infinitesimal "bi-modular" materials

Orthotropy is characterized by the existence of some symmetry planes given by preferred directions in the reference configuration $\boldsymbol{a}_i$, $i = 1, 2, 3$, with $\boldsymbol{a}_i \cdot \boldsymbol{a}_j = \delta_{ij}$, the Kronecker delta. In a system of representation given by $A = \{\boldsymbol{a}_i\}$, the relation between strains and stresses is, using Voigt notation—see for example [42]

$$\begin{bmatrix} \sigma_{11} \\ \sigma_{22} \\ \sigma_{33} \\ \sigma_{12} \\ \sigma_{23} \\ \sigma_{13} \end{bmatrix}_A = \begin{bmatrix} C_{11} & C_{12} & C_{13} & & & \\ C_{12} & C_{22} & C_{23} & & & \\ C_{13} & C_{23} & C_{33} & & & \\ & & & C_{44} & & \\ & & & & C_{55} & \\ & & & & & C_{66} \end{bmatrix}_A \begin{bmatrix} \varepsilon_{11} \\ \varepsilon_{22} \\ \varepsilon_{33} \\ 2\varepsilon_{12} \\ 2\varepsilon_{23} \\ 2\varepsilon_{13} \end{bmatrix}_A \tag{28}$$

where the following strain components are also invariants

$$\varepsilon_{ij} = \boldsymbol{a}_i \cdot \boldsymbol{\varepsilon} \cdot \boldsymbol{a}_j = \boldsymbol{a}_i \cdot \left(\sum_{k=1}^{3} \varepsilon_k \boldsymbol{N}_k \otimes \boldsymbol{N}_k \right) \cdot \boldsymbol{a}_j = \sum_{k=1}^{3} \varepsilon_k \left(\boldsymbol{a}_i \cdot \boldsymbol{N}_k \right) \left(\boldsymbol{a}_j \cdot \boldsymbol{N}_k \right) \tag{29}$$

Alternatively, because the constants C_{ij} are not easily measurable

$$\begin{bmatrix} \varepsilon_{11} \\ \varepsilon_{22} \\ \varepsilon_{33} \\ 2\varepsilon_{12} \\ 2\varepsilon_{23} \\ 2\varepsilon_{13} \end{bmatrix}_A = \begin{bmatrix} \frac{1}{Y_1} & -\frac{\nu_{21}}{Y_2} & -\frac{\nu_{31}}{Y_3} & & & \\ -\frac{\nu_{21}}{Y_2} & \frac{1}{Y_2} & -\frac{\nu_{32}}{Y_3} & & & \\ -\frac{\nu_{31}}{Y_3} & -\frac{\nu_{32}}{Y_3} & \frac{1}{Y_3} & & & \\ & & & \frac{1}{\mu_{12}} & & \\ & & & & \frac{1}{\mu_{23}} & \\ & & & & & \frac{1}{\mu_{13}} \end{bmatrix}_A \begin{bmatrix} \sigma_{11} \\ \sigma_{22} \\ \sigma_{33} \\ \sigma_{12} \\ \sigma_{23} \\ \sigma_{13} \end{bmatrix}_A \tag{30}$$

where Y_1, Y_2, Y_3, ν_{12}, ν_{31}, ν_{32}, μ_{12}, μ_{23}, μ_{13} —or alternatively the C_{ij} in Eq.(28)— are *nine independent* material constants (Young moduli, Poisson ratios and shear moduli) for which only some inequality restrictions must hold [42]. The independency of these material constants must hold regardless of our preference for the reference configuration. These nine independent constants define *nine independent deformation modes* when an incremental deformation is considered. Therefore, if a hyperelastic model is to represent a general case of orthotropy compatible with the infinitesimal case, *nine independent* functions, or nine independent function dependencies of the nine independent invariants are needed. In Eq. (30) above we could assume, for example $\nu_{12} = \nu_{23} = \nu_{13}$. In such a case, we would be eliminating two constants, and also two independent deformation modes, leaving only *seven* independent modes, and resulting in *a restricted theory*. There is nothing wrong in doing so *if that assumption is based on experimental evidence*, not in the modeler's convenience. Precisely, a usual restricted theory, based on some experimental evidence, but that only holds in average, is that soft tissues are incompressible. Then, we are eliminating the three volumetric deformation modes, imposing that the Jacobian $J = 1$, or in the infinitesimal context, the following incremental constraint:

$$\varepsilon_{11} + \varepsilon_{22} + \varepsilon_{33} = 0 \tag{31}$$

Because stress increments may be arbitrary, this constraint in turn means that the first three columns in Eq. (30) must vanish in all cases, leaving in the fully linear theory six independent constants. The three equations may be written in terms of

the complementary Poisson ratios $\nu_{ij} = \nu_{ji} Y_i / Y_j$ as

$$\left.\begin{array}{r} 1 - \nu_{12} - \nu_{13} = 0 \\ -\nu_{21} + 1 - \nu_{23} = 0 \\ -\nu_{31} - \nu_{32} + 1 = 0 \end{array}\right\} \tag{32}$$

The observable Young moduli are convenient for tests. For constitutive modelling we can alternatively use shear-like moduli μ_{11}^*, μ_{22}^*, μ_{33}^* such that, in Voigt notation

$$\begin{bmatrix} \sigma_{11} \\ \sigma_{22} \\ \sigma_{33} \\ \sigma_{12} \\ \sigma_{23} \\ \sigma_{13} \end{bmatrix}_A = [\mathbb{P}] \begin{bmatrix} 2\mu_{11}^* & & & & & \\ & 2\mu_{22}^* & & & & \\ & & 2\mu_{33}^* & & & \\ & & & \mu_{12} & & \\ & & & & \mu_{23} & \\ & & & & & \mu_{13} \end{bmatrix}_A [\mathbb{P}] \begin{bmatrix} \varepsilon_{11} \\ \varepsilon_{22} \\ \varepsilon_{33} \\ 2\varepsilon_{12} \\ 2\varepsilon_{23} \\ 2\varepsilon_{13} \end{bmatrix}_A + \begin{bmatrix} p \\ p \\ p \\ 0 \\ 0 \\ 0 \end{bmatrix} \tag{33}$$

where p is the pressure increment to be obtained from equilibrium and $[\mathbb{P}]$ is the matrix representation of the deviatoric projector tensor. In finite element implementations, it is customary to assume quasi-incompressibility incorporating a penalty function $\mathcal{U}(\ln J)$, so $Jp = \mathcal{U}'(\ln J)$ in the large strain context and $p = \kappa \varepsilon_v$ in the small strain one. As in the isotropic case, the axial terms may take different values depending on the sign of ε_{ii}, i.e.

$$\mu_{ii}^* = \begin{cases} \mu_{ii}^t \text{ if } \varepsilon_{ii} > 0 \\ \mu_{ii}^c \text{ if } \varepsilon_{ii} < 0 \end{cases}$$

The first nontrivial (nondiagonal) 3×3 box is

$$\begin{aligned} &\begin{bmatrix} \frac{2}{3} & -\frac{1}{3} & -\frac{1}{3} \\ -\frac{1}{3} & \frac{2}{3} & -\frac{1}{3} \\ -\frac{1}{3} & -\frac{1}{3} & \frac{2}{3} \end{bmatrix} \begin{bmatrix} 2\mu_{11}^* & 0 & 0 \\ 0 & 2\mu_{22}^* & 0 \\ 0 & 0 & 2\mu_{33}^* \end{bmatrix}_A \begin{bmatrix} \frac{2}{3} & -\frac{1}{3} & -\frac{1}{3} \\ -\frac{1}{3} & \frac{2}{3} & -\frac{1}{3} \\ -\frac{1}{3} & -\frac{1}{3} & \frac{2}{3} \end{bmatrix} \\ &= \frac{2}{9} \begin{bmatrix} 4\mu_{11}^* + \mu_{22}^* + \mu_{33}^* & \mu_{33}^* - 2\mu_{22}^* - 2\mu_{11}^* & \mu_{22}^* - 2\mu_{11}^* - 2\mu_{33}^* \\ \mu_{33}^* - 2\mu_{22}^* - 2\mu_{11}^* & \mu_{11}^* + 4\mu_{22}^* + \mu_{33}^* & \mu_{11}^* - 2\mu_{22}^* - 2\mu_{33}^* \\ \mu_{22}^* - 2\mu_{11}^* - 2\mu_{33}^* & \mu_{11}^* - 2\mu_{22}^* - 2\mu_{33}^* & \mu_{11}^* + \mu_{22}^* + 4\mu_{33}^* \end{bmatrix}_A \end{aligned} \tag{34}$$

which allows the immediate identification of the constants C_{ij} by direct comparison with Eq. (28). Note that we have, for example, different C_{11}^* depending on the combination of the signs of the strains ε_{11}, ε_{22} and ε_{33}. Of course the constants μ_{ii}^* can also be related to the Young moduli Y_i^*, just considering a tensile test in any axis.

Therefore, we have *nine* independent constants, namely μ_{11}^t, μ_{11}^c, μ_{22}^t, μ_{22}^c, μ_{33}^t, μ_{33}^c, μ_{12}, μ_{13}, μ_{23}, because μ_{12}, μ_{13}, μ_{23} cannot take different "tension" or "compression" values since shear strains have no physical sign.

Equation (33) implies the following approximation of the stored energy around the equilibrium reference configuration

$$\begin{aligned}\mathcal{W}(\boldsymbol{\varepsilon}, \boldsymbol{a}_1, \boldsymbol{a}_2) = \mu_{11}^* \left(\varepsilon_{11}^d\right)^2 + \mu_{22}^* \left(\varepsilon_{22}^d\right)^2 + \mu_{33}^* \left(\varepsilon_{33}^d\right)^2 \\ + 2\mu_{12} \left(\varepsilon_{12}^d\right)^2 + 2\mu_{23} \left(\varepsilon_{23}^d\right)^2 + 2\mu_{13} \left(\varepsilon_{13}^d\right)^2 + \tfrac{1}{2}\kappa\varepsilon_v^2 \end{aligned} \tag{35}$$

so

$$\boldsymbol{\sigma} = \frac{d\mathcal{W}}{d\boldsymbol{\varepsilon}} = \frac{\partial \mathcal{W}}{\partial \varepsilon_v}\frac{\partial \varepsilon_v}{\partial \boldsymbol{\varepsilon}} + \sum_{i,j}\left(\frac{\partial \mathcal{W}}{\partial \varepsilon_{ij}^d}\frac{\partial \varepsilon_{ij}^d}{\partial \boldsymbol{\varepsilon}^d}\right) : \frac{\partial \boldsymbol{\varepsilon}^d}{\partial \boldsymbol{\varepsilon}} \tag{36}$$

$$= \kappa\varepsilon_v \boldsymbol{I} + \sum_{i,j=1}^{3} 2\mu_{ij}^* \varepsilon_{ij}^d \frac{\partial \varepsilon_{ij}^d}{\partial \boldsymbol{\varepsilon}^d} : \mathbb{P} \tag{37}$$

with the structural tensor (accounting for symmetries)

$$\frac{\partial \varepsilon_{ij}^d}{\partial \boldsymbol{\varepsilon}^d} = \frac{1}{2}\left(\boldsymbol{a}_i \otimes \boldsymbol{a}_j + \boldsymbol{a}_j \otimes \boldsymbol{a}_i\right) = \boldsymbol{L}_{ij} \tag{38}$$

so

$$\boldsymbol{\sigma} = \kappa\varepsilon_v \boldsymbol{I} + \sum_{i,j=1}^{3} 2\mu_{ij}\varepsilon_{ij}^d \boldsymbol{L}_{ij} : \mathbb{P} \tag{39}$$

3.2. WYPiWYG orthotropic uncoupled model

Extending the previous discussion on large strains to orthotropy, we note that incremental infinitesimal strains can be written as

$$d_\tau \boldsymbol{\varepsilon} = \sum_{i=1}^{3} d_\tau \varepsilon_i \boldsymbol{N}_i \otimes \boldsymbol{N}_i \tag{40}$$

and they bring the following projections in the orthotropic preferred material directions

$$d_\tau \varepsilon_{ij} = \boldsymbol{L}_{ij} : d_\tau \boldsymbol{\varepsilon} = \boldsymbol{a}_i \cdot d_\tau \boldsymbol{\varepsilon} \cdot \boldsymbol{a}_j = \sum_{k=1}^{3} d_\tau \varepsilon_k \left(\boldsymbol{a}_i \cdot \boldsymbol{N}_k\right)\left(\boldsymbol{a}_j \cdot \boldsymbol{N}_k\right) \tag{41}$$

These projections are invariants—also note that eigenvalues are invariants, the director cosines $(\boldsymbol{a}_i \cdot \boldsymbol{N}_j)$ are also invariants, and operations among invariants are invariants. Director cosine invariants are also used by Shariff [3], [4]. Consider again that the deformation is computed with the principal directions fixed, see Eq. (14). Then, using the volumetric-distortion deformation decomposition and defining for convenience $\boldsymbol{N}_i^d := \boldsymbol{N}_i : \mathbb{P}$, we obtain the following logarithmic strain *invariants*

$$\begin{aligned} {}^t_0E_{ij} = \boldsymbol{a}_i \cdot {}^t_0\boldsymbol{E} \cdot \boldsymbol{a}_j &= {}^t_0E_v\delta_{ij} + \sum_{k=1}^{3} {}^t_0E^d_k \left(\boldsymbol{a}_i \cdot \boldsymbol{N}^d_k\right)\left(\boldsymbol{a}_j \cdot \boldsymbol{N}^d_k\right) \\ &= \left(\int_0^t d_\tau\varepsilon_v\right)\delta_{ij} + \sum_{k=1}^{3}\left(\int_0^t d_\tau\varepsilon^d_k\right)\left(\boldsymbol{a}_i \cdot \boldsymbol{N}^d_k\right)\left(\boldsymbol{a}_j \cdot \boldsymbol{N}^d_k\right) \end{aligned} \tag{42}$$

Again, we obtain

$${}^t_0E_{ij} = \int_0^t d_\tau\varepsilon_{ij}, \;\; {}^t_0E_v = \int_0^t d_\tau\varepsilon_v \;\; \text{and} \;\; {}^t_0E^d_{ij} = \int_0^t d_\tau\varepsilon^d_{ij} \tag{43}$$

so, for example, $d_\tau\varepsilon^d_{ij} = dE^d_{ij}$. Then, defining $\boldsymbol{L}^d_{ij} := \boldsymbol{L}_{ij} : \mathbb{P}$, at time $\tau + d\tau$, we can write

$${}^{\tau+d\tau}\boldsymbol{T} = {}^{\tau}\boldsymbol{T} + {}_\tau\kappa^{\#}\, d_\tau\varepsilon_v\boldsymbol{I} + \sum_{i,j=1}^{3} 2\, {}_\tau\mu_{ij}\, d_\tau\varepsilon^d_{ij}\, \boldsymbol{L}^d_{ij} \tag{44}$$

and integrate the stresses following the mentioned path with constant principal directions —recall that in hyperelasticity the stresses for given strains are path independent

$${}^t\boldsymbol{T} = \left(\int_0^t {}_\tau\kappa^{\#}\, d_\tau E_v\right)\boldsymbol{I} + \sum_{i,j=1}^{3}\left(\int_0^t 2\, {}_\tau\mu_{ij}\, d_\tau E^d_{ij}\right)\boldsymbol{L}^d_{ij} \tag{45}$$

As in the isotropic case, we can define the functions

$$\mathcal{U}''\left(E_v\left(\tau\right)\right) := \left.\frac{d^2\mathcal{U}}{dE_v^2}\right|_{E_v = E_v(\tau)} = {}_\tau\kappa^{\#} \equiv \kappa\left(E_v\right) \tag{46}$$

$$\omega''_{ij}\left(E^d_{ij}\left(\tau\right)\right) := \left.\frac{d^2\omega_{ij}}{dE^d_{ij}dE^d_{ij}}\right|_{E^d_{ij} = E^d_{ij}(\tau)} = 2\, {}_\tau\mu^*_{ij} \equiv 2\mu_{ij}\left(E^d_{ij}\right) \tag{47}$$

Then, accounting for symmetry, the following stored energy results in the stresses Eq. (45)

$$\begin{aligned}\Psi\left(\boldsymbol{E}\right) &= \mathcal{U}\left(E_v\right) + \mathcal{W}\left(\boldsymbol{E}^d, \boldsymbol{a}_1, \boldsymbol{a}_2\right) \\ &= \mathcal{U}\left(E_v\right) + \omega_{11}\left(E^d_{11}\right) + \omega_{22}\left(E^d_{22}\right) + \omega_{33}\left(E^d_{33}\right) + \\ &+ 2\omega_{12}\left(E^d_{12}\right) + 2\omega_{13}\left(E^d_{13}\right) + 2\omega_{23}\left(E^d_{23}\right)\end{aligned} \tag{48}$$

Of course this stored energy does not contain possible coupling terms that must vanish for infinitesimal strains around the chosen reference configuration, but this stored energy is fully compatible with the infinitesimal framework at every configuration. However, it may not fulfill the material symmetries congruency [39] because if anisotropy vanishes, the directions $\boldsymbol{a}_i$ are not defined, ω_{ii} should converge to a single $\omega-$function that, furthermore, should depend only on the three remaining invariants, namely the principal strains E^d_i. Then, to guarantee that congruency we write

$$\mathcal{W}\left(\boldsymbol{E}^d, \boldsymbol{a}_1, \boldsymbol{a}_2\right) = \mathcal{W}^{is}\left(\boldsymbol{E}^d\right) + \mathcal{W}^{or}\left(\boldsymbol{E}^d, \boldsymbol{a}_1, \boldsymbol{a}_2\right) \tag{49}$$

where $\mathcal{W}^{is}\left(\boldsymbol{E}^d\right)$ follows the Valanis-Landel decomposition. When considering both contributions, the stresses are

$$\boldsymbol{T} = \frac{d\Psi}{d\boldsymbol{E}} = \mathcal{U}'\left(E_v\right)\boldsymbol{I} + \sum_{i=1}^{3}\omega'\left(E^d_i\right)\boldsymbol{M}^d_i + \sum_{i,j=1}^{3}\omega'_{ij}(E^d_{ij})\boldsymbol{L}^d_{ij} \tag{50}$$

3.3. Discussion about coupling terms

The uncoupled Equation (48) converges to the exact infinitesimal form Eq. (35) which considers the possibility of different behavior in tension and compression, but, again, many other large strain models do so. If the form Eq. (49) is employed in the present uncoupled setting, the isotropic part contains a Valanis-Landel decomposition, whereas the anisotropic deviation from isotropy has the uncoupled form Eq. (48). In considering such decomposition, the use of logarithmic strains instead of quadratic strains is important. For instance, consider a pure shear test. Then the logarithmic strain tensor in the Cartesian system X is

$$\boldsymbol{E} = \ln \boldsymbol{U} = \int d_\tau \boldsymbol{\varepsilon} = \left[\begin{array}{cc} 0 & \ln\lambda \\ \ln\lambda & 0 \end{array}\right]_X \tag{51}$$

which has vanishing normal strains. In contrast, Green-Lagrange strains $\boldsymbol{A}$ have nonvanishing normal strains

$$\boldsymbol{A} = \frac{1}{2}\left(\boldsymbol{X}^T\boldsymbol{X} - \boldsymbol{I}\right) = \frac{\lambda^2 - 1}{(2\lambda)^2}\left[\begin{array}{cc} \lambda^2 - 1 & \lambda^2 + 1 \\ \lambda^2 + 1 & \lambda^2 - 1 \end{array}\right]_X \tag{52}$$

where $\boldsymbol{X}$ is the deformation gradient. Furthermore, during a simple shear test, A_{12} grows linearly with the "amount of shear" γ, whereas E_{12} reaches a maximum at $\gamma = 3.018$, which reflects the fact that simple shear deformations for large γ can be increasingly considered as a tensile test [37].

Obviously, coupling terms may still be present in the anisotropic contribution, and WYPiWYG formulations may include those terms [31]. However, the characterization of a material in which those terms are important requires, in general, substantial testing.

3.4. Transverse isotropic case

The transverse isotropic case, with direction 3 being the preferred direction, is obtained from the orthotropic model by setting $C_{22} = C_{11}$, $C_{23} = C_{13}$, $C_{44} = (C_{11} - C_{12})/2$ and $C_{55} = C_{66}$, or alternatively $Y_2 = Y_1$, $\nu_{32} = \nu_{31}$, $\mu_{12}^{-1} = 2(1 + \nu_{21})/Y_1$ and $\mu_{23} = \mu_{13}$, so we are left with $9 - 4 = 5$ constants. In this transverse isotropic case, Eqs. (34) and (28) give, as expected, $\mu_{11} = \mu_{22}$, $G_{12} = (C_{11} - C_{12})/2 = \mu_{11}$ and $G_{13} = C_{66} = C_{55} = \mu_{13}$ for any bulk modulus κ. In the incompressible case, the first three columns of the last equation must sum-up to zero, which result in two independent constraints which can be written in terms of Poisson ratios as

$$\left\{\begin{array}{r} 1 - \nu_{12} - \nu_{13} = 0 \\ -2\nu_{31} + 1 = 0 \end{array}\right.$$

so we are left with $5 - 2 = 3$ constants. The form of the infinitesimal "bi-modular" stored energy around a reference configuration may be written in terms of three μ_{ij}^* constants as

$$\mathcal{W}(\boldsymbol{\varepsilon}, \boldsymbol{a}_1, \boldsymbol{a}_2) = \mu_{11}^*\varepsilon_{11}^2 + \mu_{11}^*\varepsilon_{22}^2 + \mu_{33}^*\varepsilon_{33}^2 + 2\mu_{13}\varepsilon_{13}^{\#2} \tag{53}$$

where ε_{11} and ε_{22} are in-isotropic-plane principal strains (i.e. in special axes such that $\varepsilon_{12} = 0$), $\varepsilon_{33} = \boldsymbol{a}_3 \cdot \boldsymbol{\varepsilon} \cdot \boldsymbol{a}_3$, and $\varepsilon_{13}^{\#2} := \varepsilon_{23}^2 + \varepsilon_{13}^2$ is the shear invariant for all planes including the preferred direction 3 [52]. Since the moduli $\mu_{11}^*(\varepsilon)$ and $\mu_{33}^*(\varepsilon)$ may take different values for positive and negative strain arguments ε (tension-compression) we need in general 5 independent test curves. Again, in the large strain case

$$\mathcal{W}^{tr}(\boldsymbol{E}, \boldsymbol{a}_1, \boldsymbol{a}_2) = \omega_{11}(E_{11}) + \omega_{11}(E_{22}) + \omega_{33}(E_{33}) + 2\omega_{13}(E_{13}^{\#2}) \tag{54}$$

with $E_{13}^{\#2} = E_{13}^2 + E_{23}^2$ and we recover a parallel discussion. Obviously the functions need not to be symmetric, having different values in tension and compression

$$\omega_{jj}\left(E\right) \neq \omega_{jj}\left(-E\right) \ , \quad E > 0 \ , \quad j = 1, 3 \tag{55}$$

except for the function ω_{13} because the argument is always positive (meaning that shear deformations have no physical sign). Note that the consideration of the compression branches of the axial functions ω_{11} and ω_{33} is as important as the consideration of their tension branches, which is a fact that may easily explain some issues regarding the characterization of hyperelastic materials [45], [46].

The representation Eq. (53) requires a special system of representation such that $\varepsilon_{12} = 0$, which is convenient for its nonlinear extension of Eq. (54). Other systems of representation may be more convenient for the linear case. Given any other Cartesian system of representation $\{\tilde{\boldsymbol{a}}_1, \tilde{\boldsymbol{a}}_2, \tilde{\boldsymbol{a}}_3\}$ such that $\boldsymbol{a}_3 \equiv \tilde{\boldsymbol{a}}_3$, the quantities $\tilde{\varepsilon}_{11}^2 + \tilde{\varepsilon}_{22}^2 + 2\tilde{\varepsilon}_{12}^2$, $\tilde{\varepsilon}_{33}^2$ and $\tilde{\varepsilon}_{13}^{\#2} = \tilde{\varepsilon}_{13}^2 + \tilde{\varepsilon}_{23}^2$ are invariants under rotations of the preferred reference frame about the direction $\boldsymbol{a}_3 \equiv \tilde{\boldsymbol{a}}_3$, where $\tilde{\varepsilon}_{ij}$ are the corresponding cartesian components of $\boldsymbol{\varepsilon}$. Then, we can rephrase Eq. (53) in generic preferred transversely isotropic axes (i.e. with $\tilde{\varepsilon}_{12} = \tilde{\boldsymbol{a}}_1 \cdot (\boldsymbol{\varepsilon} \cdot \tilde{\boldsymbol{a}}_2)$ not necessarily zero) through

$$\mathcal{W} = \mu_{11}^2 \tilde{\varepsilon}_{11}^2 + \mu_{11} \tilde{\varepsilon}_{22}^2 + \mu_{33} \tilde{\varepsilon}_{33}^2 + 2\mu_{11} \tilde{\varepsilon}_{12}^2 + 2\mu_{13} \tilde{\varepsilon}_{13}^2 + 2\mu_{13} \tilde{\varepsilon}_{23}^2 \tag{56}$$

In Ref. [9], Section 3, the relationship between stresses and infinitesimal strains for incompressible, transversely isotropic solids is directly written in a generic preferred plane in terms of three material constants, namely

$$\mu_T \ , \quad \mu_L \ , \quad \mathcal{C}_{33} \tag{57}$$

where μ_T represents the infinitesimal shear moduli for shearing in a plane normal to the fibres, μ_L stands for the infinitesimal shear moduli for shearing in a plane along the fibres and $\mathcal{C}_{33}$ is a material constant defined in terms of μ_T and the Young's modulus in the fibre direction Y_L through

$$\mathcal{C}_{33} = Y_L - \mu_T \tag{58}$$

In our case, after a component-by-component differentiation of Eq. (56), as given in Eq. (36), we obtain

$$\tilde{\sigma}_{ij} = 2\mu_{ij} \tilde{\varepsilon}_{ij} + p \ , \quad i, j = \{1, 2, 3\} \tag{59}$$

and by direct comparison with Eqs. (12) in Ref. [9] we arrive at

$$2\mu_{11} \equiv 2\mu_T \ , \quad 2\mu_{33} \equiv \mathcal{C}_{33} \ , \quad 2\mu_{13} \equiv 2\mu_L \tag{60}$$

Hence, we can determine the strain energy constants present in Eq. (56) from a uniaxial test in the fibre direction (with modulus Y_L), a shear test with shearing in a plane normal to the fibres (with modulus $2\mu_T$) and a shear test with shearing in a plane along the fibres (with modulus $2\mu_L$), i.e.

$$\mu_{11} = \mu_T \ , \quad \mu_{33} = \frac{Y_L - \mu_T}{2} \ , \quad \mu_{13} = \mu_L \tag{61}$$

Then the linear material is fully characterized, and obviously the stress state associated with any other deformation state can be determined immediately from Eq. (36) and the corresponding boundary conditions.

The foregoing linear and nonlinear analyses show that, even though three material parameters fully define an incompressible transversely isotropic linear elastic material, we would need at least five independent material response curves in order to characterize a simple (uncoupled) nonlinear generalization of the linear model, where different behaviors in tension and compression along preferred axes are generally expected [45].

4. Some hyperelastic models consistent with the linear theory *in the reference configuration*

In Ref. [9], Murphy presented proper modifications over very popular models in the biomechanics literature so that they become compatible with the linear theory, i.e. so that they recover the infinitesimal moduli of Eq. (57) in the reference state. Evidently, compatibility with the linear theory is a desirable feature that any nonlinear model should fulfill [10, 17]. In this Section we analyze the mechanical behavior of two types of compatible models proposed by Murphy and show that, however, some of them may provide rather unexpected responses in modeling living tissues within the design range of physiological finite strains. The models that we analyze herein are the standard reinforcing model and the Humphrey-Yin model, both including the modifications proposed by Murphy in Ref. [9].

4.1. Compatible standard reinforcing model

The standard reinforcing model is widely used in the biomechanics field, see for example [47–49] among many others. The *compatible* standard reinforcing model, as

proposed by Murphy, reads

$$\mathcal{W}\left(\bar{I}_1, \bar{I}_4, \bar{I}_5\right) = \frac{\mu_T}{2}\left(\bar{I}_1 - 4\right) + \frac{Y_L + \mu_T - 4\mu_L}{8}\left(\bar{I}_4 - 1\right)^2 + \frac{\mu_T - \mu_L}{2}(2\bar{I}_4 - \bar{I}_5 - 1) \quad (62)$$

where $\bar{I}_1 = tr(\bar{\boldsymbol{C}}) = \bar{\boldsymbol{C}} : \boldsymbol{I}$ is the first principal invariant of the isochoric right Cauchy–Green deformation tensor $\bar{\boldsymbol{C}} = J^{-2/3}\boldsymbol{C}$ (with J the Jacobian and $\boldsymbol{C}$ the Cauchy–Green deformation tensor) and $\bar{I}_4 = \boldsymbol{a}_3 \cdot \bar{\boldsymbol{C}}\boldsymbol{a}_3$ and $\bar{I}_5 = \boldsymbol{a}_3 \cdot \bar{\boldsymbol{C}}^2\boldsymbol{a}_3$ are pseudo-invariants of $\bar{\boldsymbol{C}}$ including information about the deformation of the fibre direction in the referential configuration $\boldsymbol{a}_3$. This model is compatible, by construction, with the three linear responses mentioned above, i.e. those with moduli Y_L, $2\mu_T$ and $2\mu_L$, as shown in Ref. [9].

However, the physiological finite strain range of living tissues involves nonlinear responses. Hence, five independent loading cases should be correctly reproduced by the nonlinear model, or at least, it should predict realistic responses. We show in Figure 2 the respective Cauchy stresses that the material model of Eq. (62) predicts for both tension-compression uniaxial tests in directions $\boldsymbol{a}_1$ and $\boldsymbol{a}_3$, which we represent as $\sigma_1\left(E_1\right)$ and $\sigma_3\left(E_3\right)$, and an additional branch from a biaxial test in the plane $\{\boldsymbol{e}_m, \boldsymbol{e}_n\}$ including the preferred axes $\{\boldsymbol{a}_1, \boldsymbol{a}_3\}$ orientated at 45^o clockwise, as defined in Figure 1, and that we represent as $\sigma_{mm}\left(E_{mm}\right)$, with $E_{mm} = \ln\lambda$, cf. Ref. [28]. This set of tests includes the minimum number of response curves that any nonlinear model should be able to reproduce well, as we have discussed above. We consider the constants $\mu_T = 5 \times 10^{-3}\,\text{MPa}$ and $\mu_L = 29 \times 10^{-3}\,\text{MPa}$ (taken from Ref. [9]), while $Y_L = 447 \times 10^{-3}\,\text{MPa}$ taken from Ref. [49], which are realistic values within the small strain theory. When larger strains are considered, however, we can observe a minimum of $\sigma_3\left(E_3\right)$ at $E_3 = \ln\lambda_3 \approx -0.377$ (i.e. $\lambda_3 = 0.686$), which means that the material model predicts an unphysical response during the corresponding compression uniaxial test. Note that the Young modulus Y_L is positive at the reference configuration, but the Young's local modulus $(d\sigma_3/dE_3)$ vanishes at $E_3 \approx -0.377$ and becomes negative for greater compressions.

Importantly, it should be noticed that this behavior is inherently associated with the strain energy function of Eq. (62), so other softening responses may also appear in other loading situations different from the five considered herein. For example, we represent in Figure 3 the stresses $\sigma_{nn}\left(E_{mm}\right)$ and $\sigma_{mn}(E_{mm})$ that this model predicts during the pure shear test shown in Figure 1. A softening behavior can be observed again, with the stress component σ_{nn} being first negative (meaning compression), then reaching a minimum and finally becoming even positive (meaning tension). We remark, however, that this response is fully compatible with the small strain theory because $\sigma_{nn} \to -\sigma_{mm}$ and $d\sigma_{mn}/dE_{mm} \to 0$ in the small strain limit given by

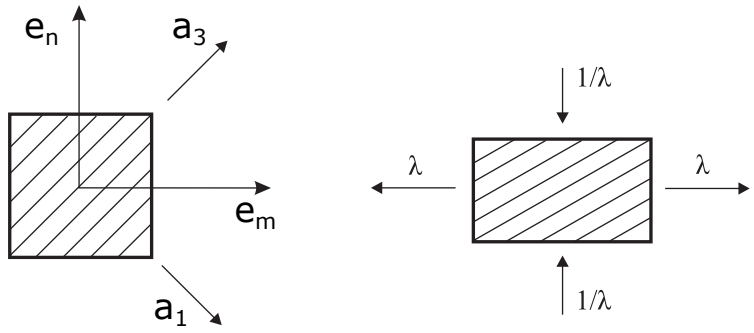

Figure 1: Specific biaxial test in axes $\{\boldsymbol{e}_m, \boldsymbol{e}_n\}$ providing a pure shear state in the logarithmic strain space in axes $\{\boldsymbol{a}_1, \boldsymbol{a}_3\}$, cf. Ref. [28]. The Lagrangian logarithmic strain tensor components in axes $\{\boldsymbol{e}_m, \boldsymbol{e}_n\}$ are $E_{nn} = -E_{mm}$ and $E_{mn} = 0$, with $E_{mm} = \ln \lambda$ and λ representing the stretch in direction $\boldsymbol{e}_m$.

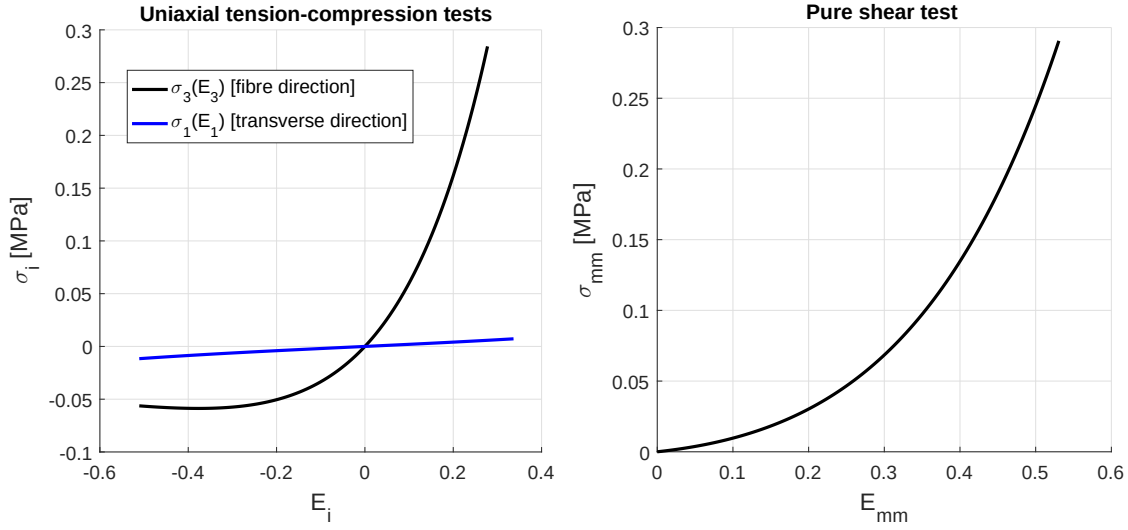

Figure 2: Modified standard reinforcing model predictions for two tension-compression uniaxial tests (left) and one axial response of the biaxial test of Figure 1 (right). We denote Cauchy stresses as σ and logarithmic strains as E.

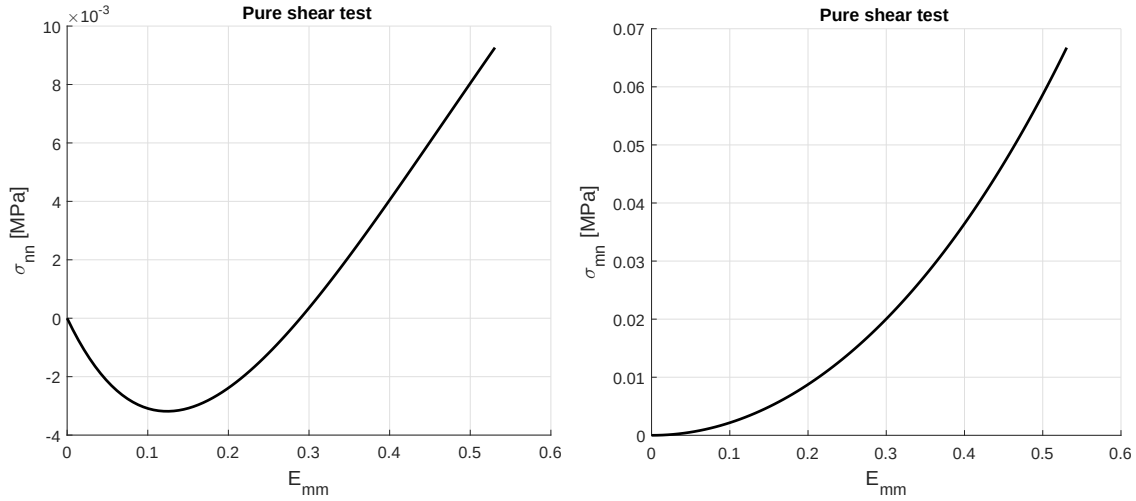

Figure 3: Additional predictions for the biaxial test of Figure 1 given by the compatible standard reinforcing model.

$E_{mm} \to \varepsilon_{mm} = 0^+$.

4.2. Compatible Humphrey-Yin model

The Humphrey-Yin model for passive cardiac tissue [50] is another very popular model in the biomechanics literature. The *compatible* Humphrey-Yin model, as proposed by Murphy, reads

$$\mathcal{W} = \frac{\mu_T}{2c_2}\left[e^{c_2(\bar{I}_1-3)}-1\right] + \frac{Y_L+\mu_T-4\mu_L}{2c_4}\left[e^{c_4(\sqrt{\bar{I}_4}-1)^2}-1\right] + \frac{\mu_T-\mu_L}{2}(2\bar{I}_4-\bar{I}_5-1) \tag{63}$$

where c_2 and c_4 are additional material constants, which inclusion in the model will prove very convenient. This model is compatible, by construction, with the three linear responses in the reference configuration mentioned above [9].

We show in Figure 4 the respective Cauchy stresses that the material model of Eq. (63) predicts for both tension-compression uniaxial tests and for the biaxial test (only one axial curve). The remaining material parameters are taken from Ref. [50]: $c_2 = 9.448$ and $c_4 = 65.86$. The predictions of the five required branches may be considered realistic in this case, which is a consequence of the fact that the additional parameters in Eq. (63) can be computed as to fit the material finite strain response within the physiological range of the living tissue being characterized.

In addition, we represent in Figure 5 the stresses $\sigma_{nn}\,(E_{mm})$ and $\sigma_{mn}(E_{mm})$ that this model predicts during the pure shear test. We observe also that all the stress

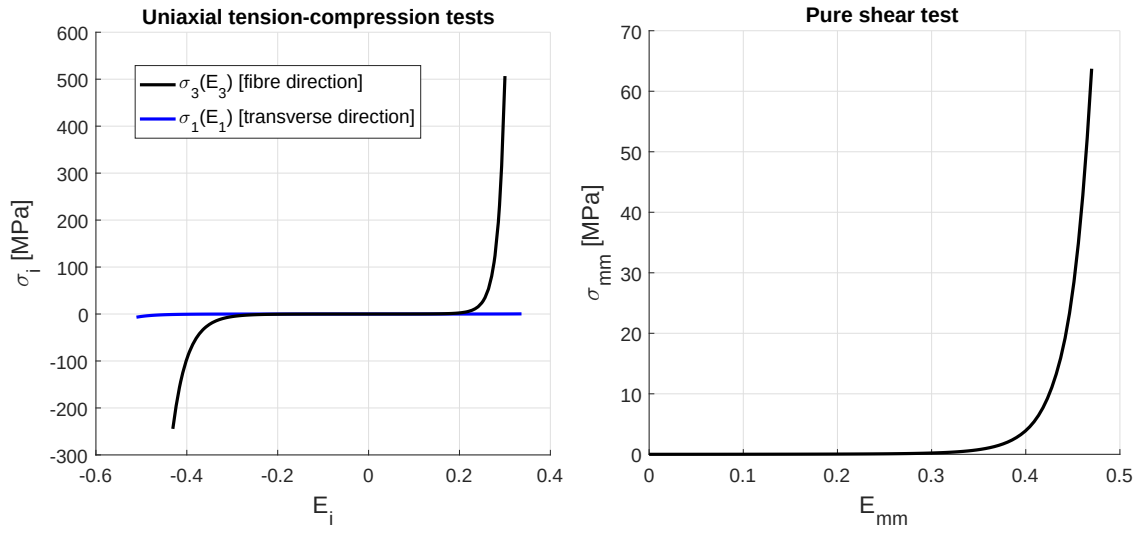

Figure 4: Modified Humphrey–Yin model predictions for two tension-compression uniaxial tests (left) and one axial response of the biaxial test of Figure 1 (right). We denote Cauchy stresses as σ and logarithmic strains as E.

responses for this boundary value problem follow the exponential tendency of the previous curves and that they may perfectly be considered realistic. We note again that $\sigma_{nn} \to -\sigma_{mm}$ and $d\sigma_{mn}/dE_{mm} \to 0$ for $E_{mm} \to 0^+$.

However, it should be taken into consideration that the role of the material constants Y_L, μ_T and μ_L in Eq. (63) is to ensure compatibility with the linear theory at the reference configuration, but not at all possible deformed configurations (as discussed above for the standard reinforcing model), so only the remaining two constants in Eq. (63), i.e c_2 and c_4, can be used to provide a good fit with experimental data over the physiological range of strain. Therefore, the model of Eq. (63) proposed in [9], with only two free constants remaining to be modulated, cannot generally reproduce the shapes of five independent deformation modes simultaneously, unless the specific soft tissue material behaves as the analytical model of Eq. (63) predicts, as it happens specifically for myocardium, as shown in Ref. [50].

5. Compatibility with the infinitesimal theory *at any arbitrary configuration*

We have seen in the previous sections that full compatibility with the small strain theory at the reference configuration (i.e. three independent constants are recovered) and additional compatibility with the infinitesimal incremental theory at finite strains

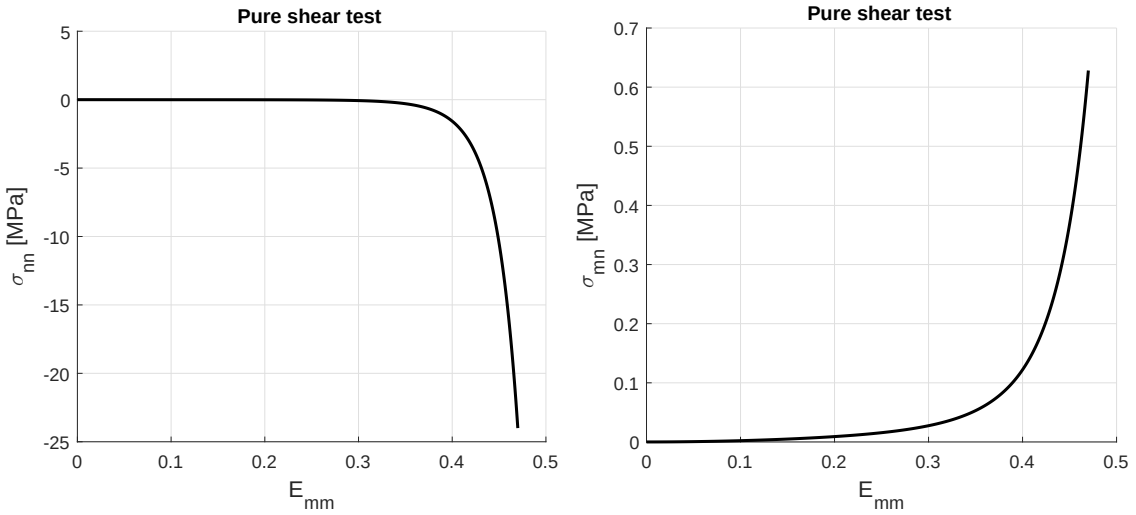

Figure 5: Additional predictions for the biaxial test of Figure 1 given by the compatible Humphrey–Yin model.

(i.e. five independent branches can be reproduced independently in the most simple case addressed herein) are very different issues. In this respect, we have shown that the former does not imply the latter. We show next that the latter includes the former as a particular case, as one could expect.

We consider in this section the uncoupled incompressible transversely isotropic WYPiWYG model [28, 51, 52]. As a first main difference with the previous models, the model of Eq. (54) requires five independent material response curves to be determined, which include the compression branches of both uniaxial tests (or other equivalent experimental curves), see discussions in Refs. [45] and [30]. If some of these experimental data are not available for the material at hand, then they must be assumed as realistically as possible before determining the strain energy function (e.g. some kind of symmetry [54] or stability criteria [28] may be considered beforehand for uniaxial compression data). This way we prevent unexpected results given a posteriori by the model, see Ref. [17] for other plausible hypothesis over (unknown) transverse strains based on additional experimental evidence [55].

A second important difference with the previous models is that the model of Eq. (54) can be exactly and uniquely determined from the five experimental curves being prescribed [52] (cf. also Ref. [17] in the context of orthotropic materials). In other words, once the model is calculated using the WYPiWYG determination procedure, the given experimental data set is exactly reproduced. As a direct consequence, the model of Eq. (54) determined by the WYPiWYG procedure is compatible, by

construction and determination, with the most simple (uncoupled) finite strain case addressed herein, because at least five independent deformation modes are captured within the finite strain regime. Furthermore, compatibility with the small strain theory is directly obtained as a particularization of the finite strain model to the small strain limit, with three independent moduli being captured at the reference state as a result.

In what follows, we will consider as if the small-strain-compatible standard reinforcing and the Humphrey–Yin models addressed by Murphy were actual materials. From the predictions of these models for some "experimental" tests, we will determine the corresponding models of the type Eq. (54) that exactly capture those tests by applying the WYPiWYG determination procedure. The corresponding infinitesimal compatibility at all finite strain levels is obtained in each case. Small strain compatibility at the reference state is directly guaranteed as a result. Of course, the same situation would be obtained if the prescribed data would correspond to an actual material. Finally, we will analyze the differences between models in general loading situations.

5.1. Capturing the modified standard reinforcing model

Consider the analytical predictions under both uniaxial tests and a pure shear test given by the standard reinforcing model shown in Figure 2. We prescribe these curves as input *experimental* data in order to determine the strain energy function of Eq. (54) using the WYPiWYG determination procedure. We show in Figure 6 the exact predictions given by the computed strain energy for the five different branches used to determine our model —cf. Fig. 2.

We show in Figure 7 additional predictions that our computed WYPiWYG model gives for other different tests performed with the standard reinforced model, which were not previously employed in the determination of our WYPiWYG stored energies. In particular, we can observe in Figure 7 that our computed model gives exactly the same predictions as the reinforcing model of Section 4.1 during other biaxial tests. Note that all the shown curves relate to each other through a vertical translation, because in preferred axes, the stresses obtained from both models are uncoupled in terms of the preferred components of the logarithmic strain tensor. In fact, this is the same effect obtained when using the Valanis-Landel decomposition in isotropic materials, and we note that it is a desirable feature if there are not sufficient experimental data to be able to adequately determine the possible coupling terms because, at least, the obtained response for these deformation modes can be qualitatively predicted by the modeler.

However, the predictions given by our computed model and those given by the

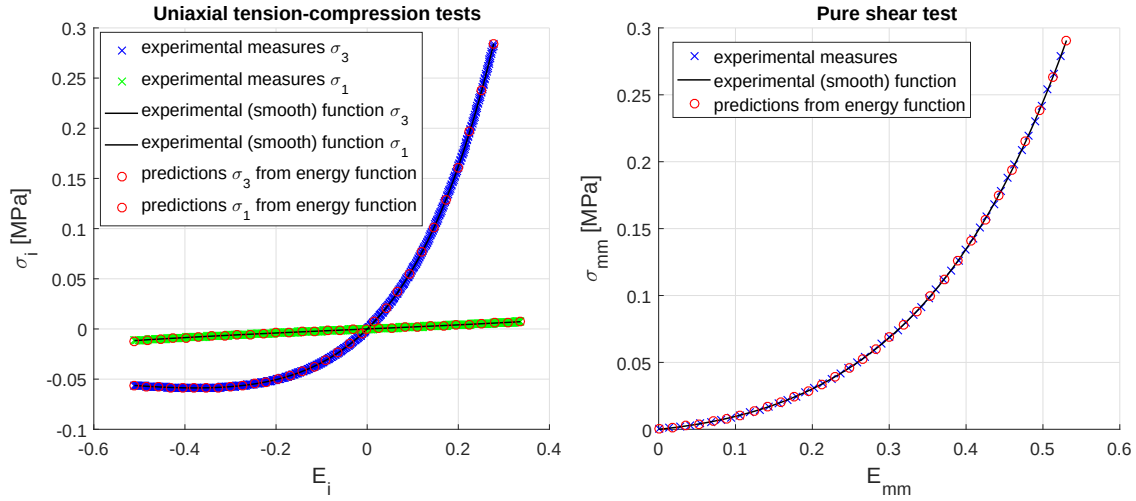

Figure 6: WYPiWYG model predictions of the standard reinforcing model "experimental data" of Figure 2.

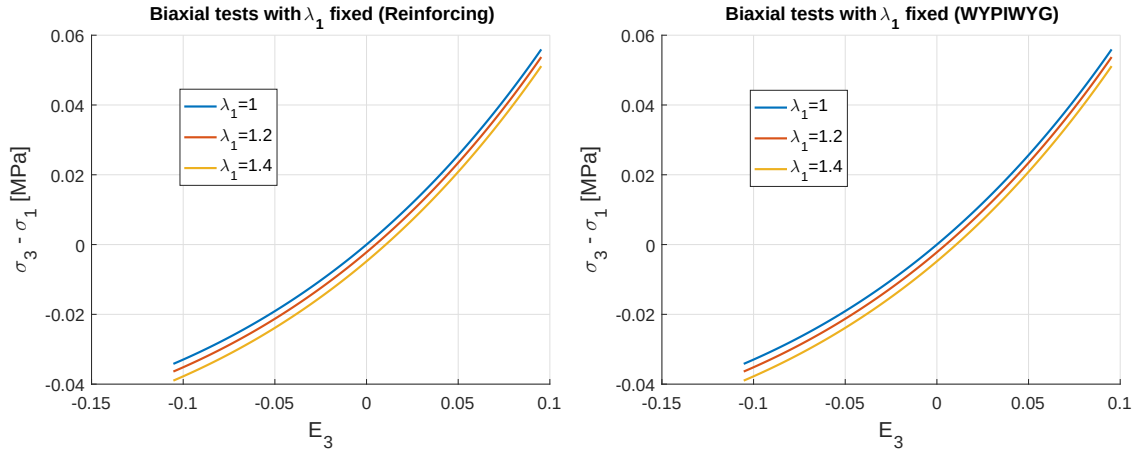

Figure 7: Additional predictions of the compatible standard reinforcing model and its associated WYPiWYG model for tension-compression tests in direction $\boldsymbol{a}_3$ with different fixed transverse strains in direction $\boldsymbol{a}_1$. A plane stress condition is considered in the remaining direction.

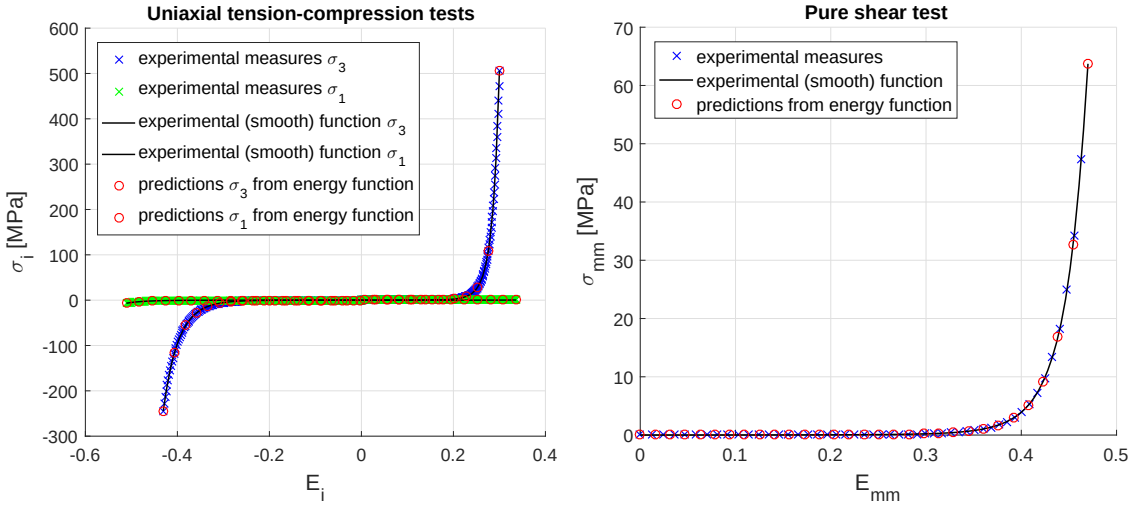

Figure 8: WYPiWYG model predictions of the Humphrey–Yin model "experimental data" of Figure 2.

associated standard reinforcing model are very different for the remaining curves $\sigma_{nn}\,(E_{mm})$ and $\sigma_{mn}(E_{mm})$ of the pure shear test shown in Figure 1. As explained in Ref. [28], the model of Eq. (54) predicts a pure shear state of Cauchy stresses in the preferred axes $\{\boldsymbol{a}_1, \boldsymbol{a}_3\}$ and as a result we obtain the stress components $\sigma_{nn} = -\sigma_{mm}$ and $\sigma_{mn} = 0$ in the test axes $\{\boldsymbol{e}_m, \boldsymbol{e}_n\}$. These predictions, with $\sigma_{mm}(E_{mm})$ shown in Figure 6, are to be compared with those shown in Figure 2. Of course, if a nonsymmetric contribution is added for the isotropic part, see Eq. (49), a Poynting effect is obtained, see Appendix.

5.2. Capturing the modified Humphrey-Yin model

Consider the analytical predictions under both uniaxial tests and a pure shear test given by the modified Humphrey–Yin model shown in Figure 4. We prescribe these curves as input *experimental* data in order to determine the strain energy function of Eq. (54) using the WYPiWYG determination procedure. We show in Figure 8 the exact predictions given by the computed strain energy for the five different branches used to determine our model, cf. Fig.4.

We show in Figure 9 additional predictions that our computed model gives for other additional tests not employed in the determination of the WYPiWYG stored energy. In this case, we can observe in Figure 9 that, during biaxial tests, our computed model gives very different predictions than those of the Humphrey–Yin model of Section 4.2 *if large transverse strains are present.* These differences are due

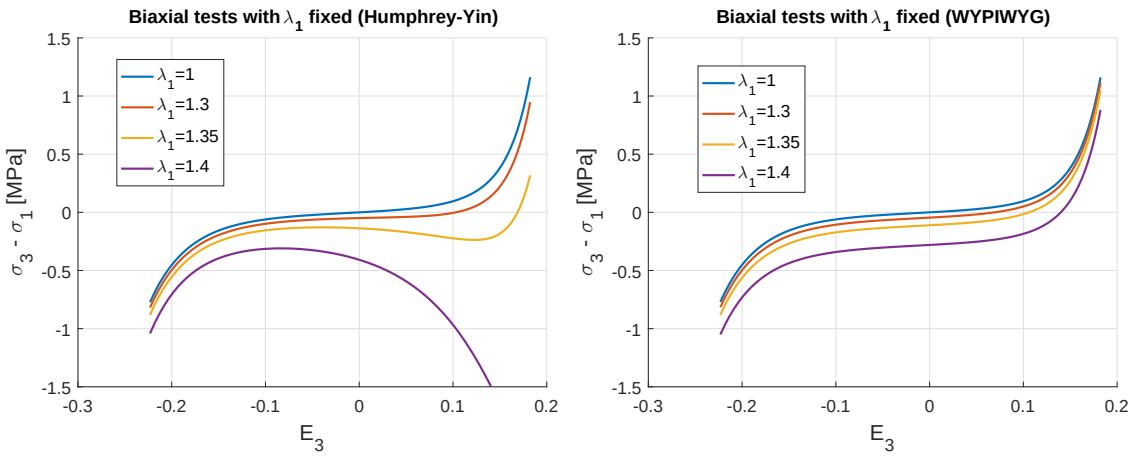

Figure 9: Additional predictions of the compatible Humphrey–Yin model and its associated WYPiWYG model for tension-compression tests in direction $\boldsymbol{a}_3$ with different fixed transverse strains in direction $\boldsymbol{a}_1$. A plane stress condition is considered in the remaining direction.

to the fact that the stresses, in preferred axes, that derive from the strain energy of Eq. (54) are uncoupled in terms of the preferred components of the logarithmic strain tensor, while the same stress components that derive from the strain energy of Eq. (63) present specific strain couplings through the exponential term $e^{c_2(\bar{I}_1-3)}$ giving a deviatoric decay in $\sigma_3 - \sigma_1$ for some values of λ_1. Whether the material under study does or does not present this possible coupling response could only be verified against additional biaxial experimental data.

Finally, the predictions given by our computed model for the remaining curves $\sigma_{nn}\,(E_{mm})$ and $\sigma_{mn}(E_{mm})$ of the pure shear test shown in Figure 1 (i.e. $\sigma_{nn} = -\sigma_{mm}$ and $\sigma_{mn} = 0$ with $\sigma_{mm}(E_{mm})$ shown in Figure 8) and those given by the associated Humphrey–Yin model (Figure 5) are also different in this case, but all of them are arguably more realistic than those given by the reinforcing model (Figure 3).

6. Non-homogeneous finite element analysis

In this section we compare the stress field predictions given by the analytical models addressed above in specific non-homogeneous cases with the respective stress field predictions obtained with the uncoupled WYPiWYG models that have been determined above from the analytical models. We analyze the axial elongation of a rectangular plate with a hole under a plane strain condition for different orientations of the anisotropic direction.

The plate has initial dimensions of $l_0 \times h_0 = 32 \times 16\,\mathrm{mm}^2$ and an inner hole of

radius $r_0 = 4\,\text{mm}$. The finite element 2D mesh consists of mixed u/p finite elements 9/3 (Q2/P1) with full integration [43]. The material parameters are the same used in the previous sections. We perform the finite element simulations with the finite element analysis software ADINA [53], where the different hyperelastic models have been programmed through user-defined material subroutines. In these general non-homogeneous cases, a large variety of loading conditions and deformation levels at different integration points are present, so the comparison between model predictions is much richer than using only homogeneous tests.

6.1. Standard Reinforcing Model

In this example we perform three finite element simulations using the modified standard reinforcing model of Section 4.1, one per each orientation $\alpha = \{0^o, 60^o, 90^o\}$ of the preferred direction $\boldsymbol{a}_3$ with respect to the horizontal axis of the plate. A horizontal displacement of 3.2 mm is applied in each case in four proportional steps. This displacement corresponds to a 10% average deformation, although the plate will undergo much larger strains in the central hole passing area, as we see below. Subsequently, analogous simulations are performed using the respective WYPiWYG material model of Section 5.1 which, recall, has been determined from the five independent responses given by the reinforcing model addressed above.

The results obtained with both models (deformed configurations and von Mises stresses) are shown in Figure 10. At small strains the predictions of both models are almost identical by consistency with the infinitesimal theory at the reference configuration, so we only show the comparisons at the maximum attained deformation of the plate (far away from the reference configuration). We can observe that the outcomes for the orientation of 0^o are almost identical to each other. The deformed meshes and von Mises stress distributions for the simulations at 60^o, which undergo the corresponding angular distortion, are very similar as well. However, the effective stresses predicted by the WYPiWYG model are almost twice as much as the ones predicted by the associated standard reinforcing model. This can be explained by the very different (partial) responses that both models predict for the pure shear test of Figure 1. Indeed, even though the fibres are oriented at 45^o in Figure 1, a similar ratio of von Mises stresses between both models is obtained in that case. For example, for the standard reinforcing model curves in Figures 2 (right) and 3, with $\sigma_{mm} = 0.25\,\text{MPa}$, $\sigma_{nn} = 0.008\,\text{MPa}$ and $\sigma_{mn} = 0.06\,\text{MPa}$ at $E_{mm} = 0.5$

$$(\sigma_{eff})_{\text{SR}|45^o} = \sqrt{\frac{(\sigma_{mm} - \sigma_{nn})^2 + \sigma_{mm}^2 + \sigma_{nn}^2 + 6\sigma_{mn}^2}{2}} = 0.267\,\text{MPa} \qquad (64)$$

The same calculation for the associated WYPiWYG model in Figure 6, with $\sigma_{mm} =$

0.25 MPa, $\sigma_{nn} = -\sigma_{mm}$ MPa and $\sigma_{mn} = 0$ (i.e. a pure shear stress state) at $E_{mm} = 0.5$, gives

$$(\sigma_{eff})_{\text{WYPiWYG}|45^o} = \sqrt{3}\sigma_{mm} = 0.433\,\text{MPa} \tag{65}$$

The ratio between both predictions is

$$\frac{(\sigma_{eff})_{\text{WYPiWYG}|45^o}}{(\sigma_{eff})_{\text{SR}|45^o}} = 1.621 \tag{66}$$

Finally, some differences can also be noted in the simulations for the orientation $\alpha = 90^o$. However, an interesting feature of the WYPiWYG models can be emphasized in this last case. We can see in Figure 11 that in this last case ($\alpha = 90^o$), the analytical standard-reinforced model runs into a strain localization phenomenon in the central passing area of the plate, which is in accordance with the stationary point (i.e. degradation of the elastic stiffness, see Ref. [56]) shown in Figure 2. Remarkably, the associated WYPiWYG model is able to qualitatively reproduce that characteristic behavior of the standard reinforcing model addressed herein, see Figure 11.

6.2. Humphrey-Yin model

In this example we perform the same analyses than in the previous example, but in this case with the Humphrey–Yin model of Section 4.2 and its associated WYPiWYG model addressed in Section 5.2. The results for the maximum deformation level are shown in Figure 12. Again, we can observe that similar predictions are obtained with both models for the orientations $\alpha = 0^o$ and $\alpha = 90^o$. For the orientation $\alpha = 60^o$, where the shear behavior is predominant, the deformed configurations and stress maps predicted by both models are also in very good agreement, but the effective stresses predicted by the WYPiWYG model are again higher (approx. 50%) than the ones predicted by the Humphrey–Yin model. The reason for that difference is the same one explained above for the reinforcing model, see Figures 4 (right) and 5. Finally, we can see in Figure 13 that in this case the transverse strains do not localize, compare with Figure 11. The reason is apparent when comparing Figures 2 (standard reinforcing model) and 4 (Humphrey–Yin model).

7. Conclusions

Many models for anisotropic hyperelasticity employed in soft tissues do not recover the infinitesimal theory in the limit. Some modifications have been recently proposed to accommodate those models to the infinitesimal theory in the reference

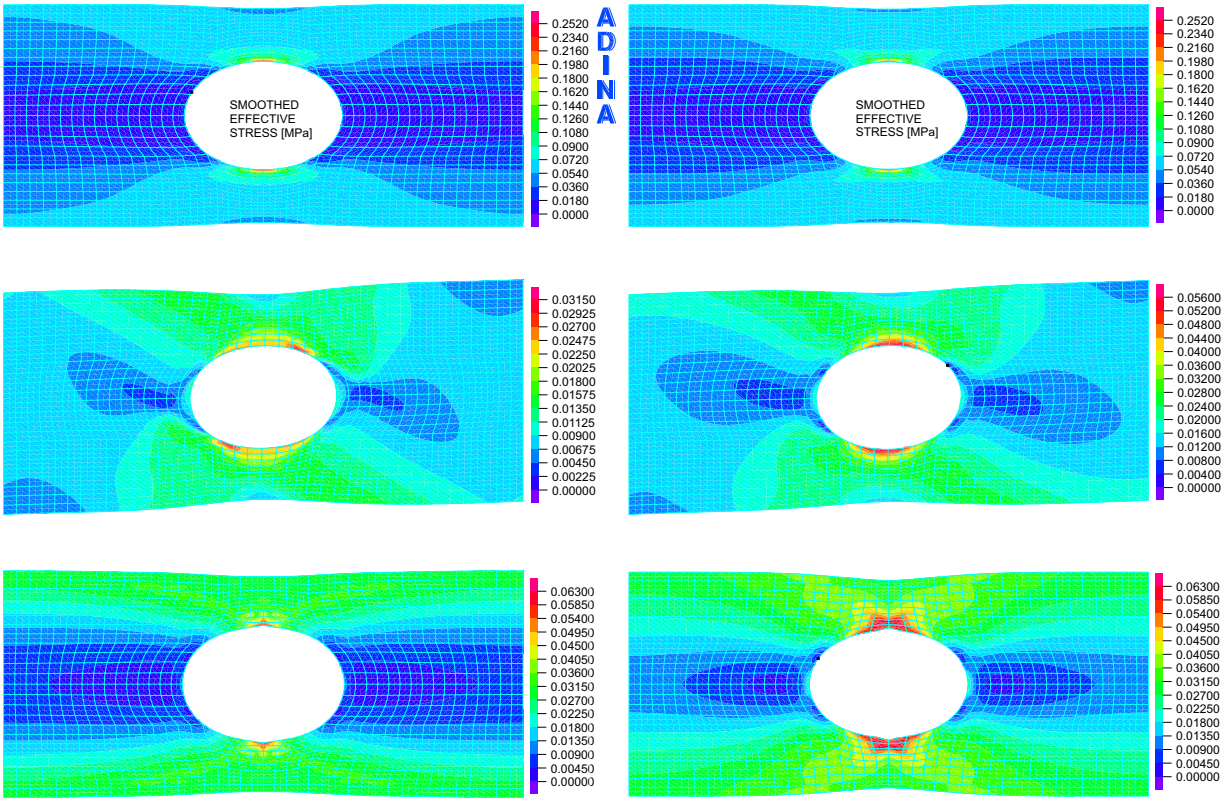

Figure 10: Finite element analyses of the horizontal elongation of a plate with a central hole and perfectly lubricated grips. Left: simulations with the standard reinforcing model of Section 4.1. Right: simulations with the corresponding WYPiWYG model of Section 5.1. Top: $\alpha = 0^o$. Middle: $\alpha = 60^o$. Bottom: $\alpha = 90^o$. The angle α indicates the orientation of the anisotropic direction $\boldsymbol{a}_3$ with the horizontal.

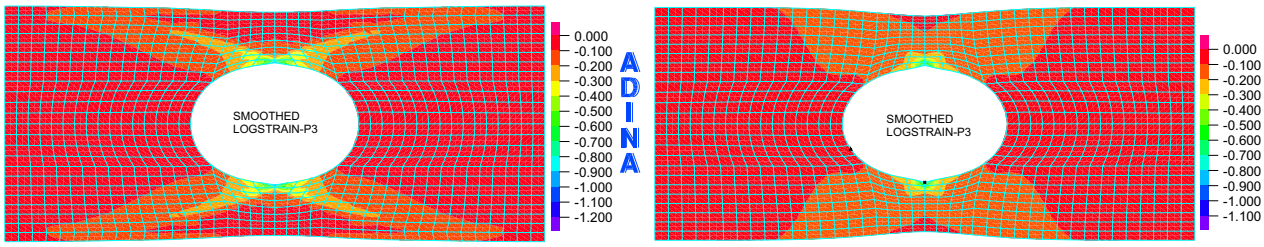

Figure 11: Left: transverse strain localization undergone by the compatible standard reinforcing model in the case $\alpha = 90^o$. Right: transverse strain localization predicted by the associated WYPiWYG model in the case $\alpha = 90^o$. Lowest principal logarithmic strains are shown in both meshes.

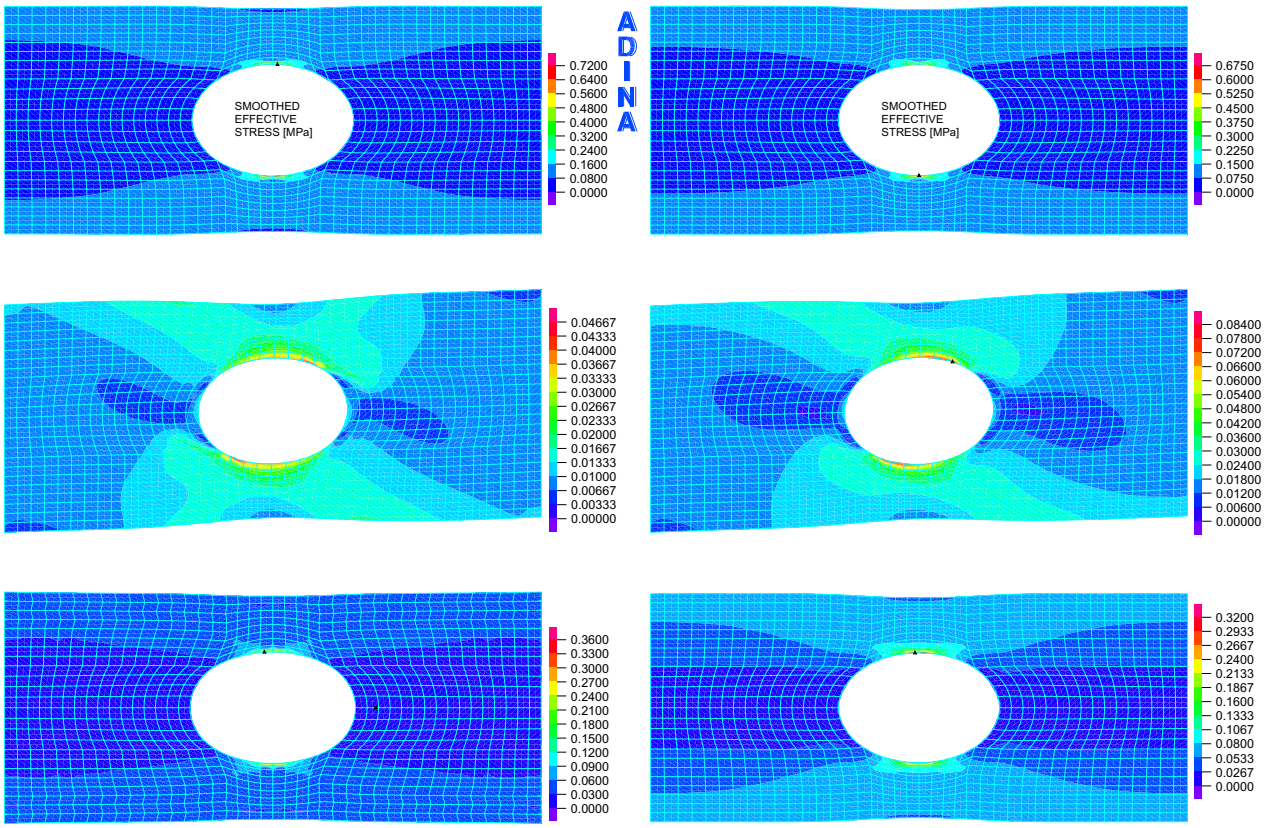

Figure 12: Finite element analyses of the horizontal elongation of a plate with a central hole and perfectly lubricated grips. Left: simulations with the Humphrey–Yin model of Section 4.2. Right: simulations with the corresponding WYPiWYG model of Section 5.2. Top: $\alpha = 0^o$. Middle: $\alpha = 60^o$. Bottom: $\alpha = 90^o$. The angle α indicates the orientation of the anisotropic direction $\boldsymbol{a}_3$ with the horizontal.

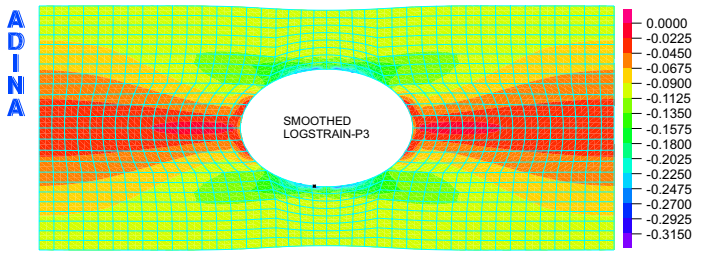

Figure 13: Lowest principal logarithmic strains predicted by the WYPiWYG model, determined from the Humphrey–Yin model, in the case $\alpha = 90^o$.

configuration. Here, we discussed the recovery of the infinitesimal theory for every incremental deformation at any deformed configuration. We show that WYPiWYG formulations are compatible with the infinitesimal theory at any deformation level and that they are capable of capturing the main aspects of both homogeneous and nonhomogeneous deformations in anisotropic solids at large strains.

Acknowledgments

Partial financial support for this work has been given by grant DPI2015-69801-R from the Dirección General de Proyectos de Investigación of the Ministerio de Economía y Competitividad of Spain. EDR acknowledges the funding for a stay at the UPM, Progetto di internazionalizzazione dei corsi di studio from COINOR-Università Degli Studi di Napoli Federico II. FJM also acknowledges the support of the Department of Mechanical and Aerospace Engineering of University of Florida during the sabbatical period in which part of this paper was performed, and that of Ministerio de Educación, Cultura y Deporte of Spain for the financial support for that stay under grant PRX15/00065. The ADINA program license used for this work has been a courtesy of ADINA R&D to the UPM.

A. Appendix: Analysis of the Poynting effect

The Poynting effect in nonlinear materials has been addressed recently in a relevant number of publications, see for example [58], [59], [61], [62], [63] and therein references. In this appendix we do not perform a detailed analysis of the Poynting effect in general models, which can be found in the previous references, but a brief analysis of the Poynting effect in shear tests in materials following our bi-linear infinitesimal formulation and materials using the uncoupled decompositions which we usually employ in WYPiWYG hyperelasticity. Some relevant conclusions may still be obtained using these simple formulations, as for example, that isotropic, infinitesimal materials may also present both a positive and a negative Poynting effect.

A.1. Bi-modular isotropic materials

In a shear test $\varepsilon_v = 0$ and

$$[\boldsymbol{\varepsilon}]_X = \begin{bmatrix} 0 & \gamma/2 & \\ \gamma/2 & 0 & \\ & & 0 \end{bmatrix} \Longrightarrow [\boldsymbol{\varepsilon}]_N = \begin{bmatrix} \gamma/2 & & \\ & -\gamma/2 & \\ & & 0 \end{bmatrix} \tag{67}$$

where $[\boldsymbol{\varepsilon}]_X$ is the matrix representation in the usual Cartesian system and $[\boldsymbol{\varepsilon}]_N$ is the matrix representation in the principal strain directions. Then the fictitious stress tensor in Eq. (7) is

$$\left[\boldsymbol{\sigma}^{|d}\right]_N = \begin{bmatrix} \mu^t\gamma & 0 & 0 \\ 0 & -\mu^c\gamma & 0 \\ 0 & 0 & 0 \end{bmatrix} \tag{68}$$

so the stress tensor is

$$\{\boldsymbol{\sigma}\}_N = \begin{bmatrix} \frac{2}{3} & -\frac{1}{3} & -\frac{1}{3} \\ -\frac{1}{3} & \frac{2}{3} & -\frac{1}{3} \\ -\frac{1}{3} & -\frac{1}{3} & \frac{2}{3} \end{bmatrix} \begin{Bmatrix} \mu^t\gamma \\ -\mu^c\gamma \\ 0 \end{Bmatrix} = \begin{Bmatrix} \frac{1}{3}\gamma\mu^c + \frac{2}{3}\gamma\mu^t \\ -\frac{2}{3}\gamma\mu^c - \frac{1}{3}\gamma\mu^t \\ \frac{1}{3}\gamma\mu^c - \frac{1}{3}\gamma\mu^t \end{Bmatrix}$$

where $\{\boldsymbol{\sigma}\}_N$ indicates the nonvanishing axial terms of the Voigt notation in principal directions, and

$$[\boldsymbol{\sigma}]_X = \begin{bmatrix} \frac{1}{3}\mu^a\gamma & \mu^s\gamma & \\ \mu^s\gamma & \frac{1}{3}\mu^a\gamma & \\ & & -\frac{2}{3}\mu^a\gamma \end{bmatrix} \tag{69}$$

is the matrix representation in the working system of representation. We have defined the "symmetric" and "antisymmetric" moduli as

$$\mu^s = \frac{1}{2}\left(\mu^t + \mu^c\right) \quad \text{and} \quad \mu^a = \frac{1}{2}\left(\mu^t - \mu^c\right) \tag{70}$$

so

$$\mu^t = \mu^s + \mu^a \quad \text{and} \quad \mu^c = \mu^s - \mu^a \tag{71}$$

Then, we obtain the effective shear modulus $G \equiv \mu^s$, and we have the following normal and shear stresses in the shearing plane

$$\sigma_n = \tfrac{1}{3}\mu^a \tag{72}$$

$$\tau_n = \mu^s\gamma \tag{73}$$

The first one, σ_n, represents the Poynting effect. In soft tissues, it is to be expected that $\mu^t > \mu^c$, so the stress of the Poynting effect is positive in such cases (a negative Poynting effect, see [59]). If $\mu^c > \mu^t$ the stress of the Poynting effect is negative (a positive Poynting effect [59]). Note that if $\mu^c = -\mu^t$ (a V-like $\omega'-$function) the material does not show apparent pure shear stiffness because $G = 0$, but it shows a Poynting effect because $\sigma_n = \frac{1}{3}\mu^t\gamma$. Furthermore, negative μ^c values are required for cases with low shear stiffness, when $G < \mu^t/2$.

The previous expressions are imposing a zero pressure and zero dilatation, and

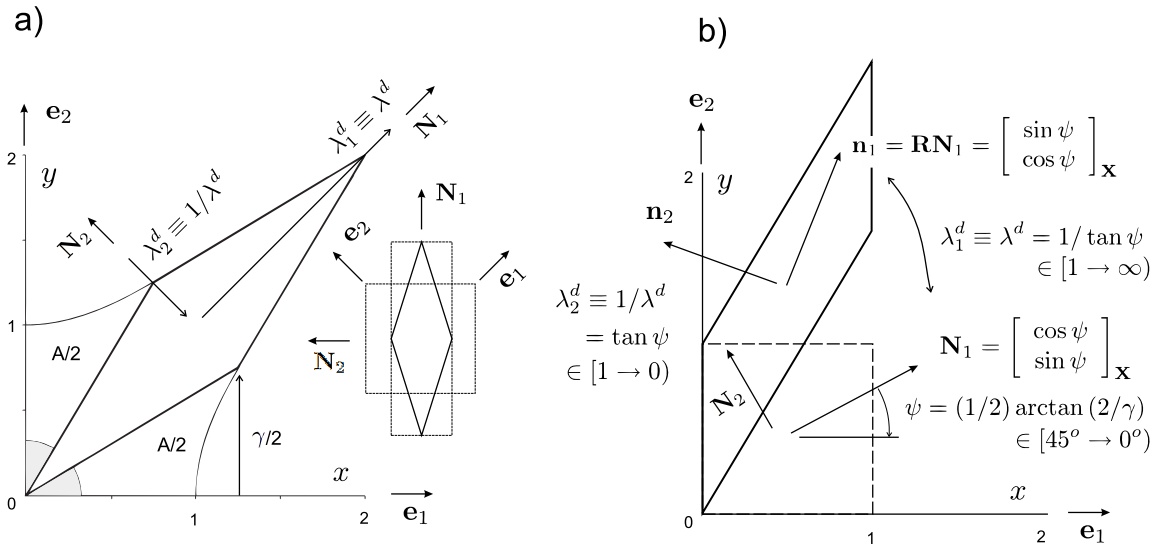

Figure 14: Quantities involved in the shear tests. a) Pure shear test. b) Simple shear test

as a result $\sigma_z = -\frac{2}{3}\mu^a\gamma \neq 0$. Another option is to enforce $\sigma_z = 0$, which results in $p = \frac{2}{3}\mu^a\gamma$, and

$$[\boldsymbol{\sigma}]_X = \begin{bmatrix} \mu^a\gamma & \mu^s\gamma & \\ \mu^s\gamma & \mu^a\gamma & \\ & & 0 \end{bmatrix} \tag{74}$$

The dilatation is $\varepsilon_v = p/\kappa^{\#} = \frac{2}{3}\left(\mu^a/\kappa^{\#}\right)\gamma$, where $\kappa^{\#}$ depends on the sign of the Poynting effect $\mu^a\gamma$. Remarkably, the shear test may be employed to determine both μ^s and μ^a (and hence μ^t and μ^c) if both shear and normal stresses are measured in the shearing plates.

A.2. Large strain isotropic Valanis-Landel models

At large strains, the pure shear test and the simple shear tests are different, see Figure 14, because the latter implies a rotation of the principal directions of deformation.

A.2.1. Pure shear test

Using the definitions

$$w^s(E) := \tfrac{1}{2}\left[\omega'(E) - \omega'(-E)\right] \quad \text{and} \quad w^a(E) := \tfrac{1}{2}\left[\omega'(E) + \omega'(-E)\right]$$

The pure shear test at large strains is similar in the logarithmic strains context as that in small strains. In this isochoric test, the principal directions remain fixed. It is straightforward to verify that —cf. Eq. (69)

$$[\boldsymbol{\sigma}]_X = [\boldsymbol{T}]_X = \begin{bmatrix} \frac{1}{3}w^a(E) & w^s(E) & \\ w^s(E) & \frac{1}{3}w^a(E) & \\ & & -\frac{2}{3}w^a(E) \end{bmatrix} \tag{75}$$

with $E = \ln\lambda = A$, where A is the sum of all dimensionless area distortions, see Fig. 14a (the *incremental* area distortion is a proper definition of the *incremental* infinitesimal shear strain, see [37]). If the stored energy term $\omega(E)$ is symmetric (even) in E, then $\omega'(E)$ is odd, and $\omega'(E) = -\omega'(-E)$, so there is no Poynting effect, and $\sigma_{12} = \omega'(E)$. Then, a similar discussion is found as in the infinitesimal case.

A.2.2. Simple shear test

At any given instant, the simple shear test is given by the following deformation gradient expressed in the cartesian system $X = \{\boldsymbol{e}_i\}$ of shearing plane/direction [57]—note that for simplicity in the derivation we uncouple the volumetric component

$$\boldsymbol{X} = J^{1/3} \begin{bmatrix} 1 & 0 & \\ 2/\tan(2\psi) & 1 & \\ & & 1 \end{bmatrix}_X \tag{76}$$

with the polar decomposition

$$\boldsymbol{X} = \begin{bmatrix} \sin 2\psi & -\cos 2\psi & 0 \\ 2\frac{\sin 2\psi}{\tan 2\psi} - \cos 2\psi & \frac{1+\cos^2 2\psi}{\sin 2\psi} - 2\frac{\cos 2\psi}{\tan 2\psi} & 0 \\ 0 & 0 & 1 \end{bmatrix} \begin{bmatrix} \frac{1+\cos^2(2\psi)}{\sin 2\psi} & \cos 2\psi & 0 \\ \cos 2\psi & \sin 2\psi & 0 \\ 0 & 0 & 1 \end{bmatrix}_X J^{1/3} \tag{77}$$

where J is the Jacobian determinant of the deformation, $\gamma = 2/\tan(2\psi) \in [0 \to \infty)$ is the so-called "amount of shear", and $\psi = (1/2)\arctan(2/\gamma) \in [\pi/4 \to 0)$ is the angle between the principal material direction associated with the tensile stretch $\lambda^d = 1/\tan(\psi) \in [1, \infty)$ and the shearing plane direction, see Figure 14. Then, in the shearing plane $\boldsymbol{N}_1 = \begin{bmatrix} \cos\psi & \sin\psi \end{bmatrix}_X^T$, $\boldsymbol{N}_2 = \begin{bmatrix} -\sin\psi & \cos\psi \end{bmatrix}_X^T$ and

$$\boldsymbol{N}_1 \otimes \boldsymbol{N}_1 = \begin{bmatrix} \cos^2\psi & \cos\psi\sin\psi \\ \cos\psi\sin\psi & \sin^2\psi \end{bmatrix}_X \tag{78}$$

$$\boldsymbol{N}_2 \otimes \boldsymbol{N}_2 = \left[\begin{array}{cc} \sin^2\psi & -\cos\psi\sin\psi \\ -\cos\psi\sin\psi & \cos^2\psi \end{array} \right]_X \tag{79}$$

The logarithmic strain tensor in the shearing plane is

$$\boldsymbol{E} = (\ln J)\,\boldsymbol{I} - \ln(\tan\psi) \left[\begin{array}{ccc} \cos(2\psi) & \sin(2\psi) & \\ \sin(2\psi) & -\cos(2\psi) & \\ & & 0 \end{array} \right]_X \tag{80}$$

Defining $E^d = \ln\lambda^d = \ln(1/\tan\psi) = -\ln(\tan\psi) > 0$, the stresses are

$$\begin{aligned} \boldsymbol{T} &= \mathcal{U}'(\ln J)\,\boldsymbol{I} + \mathbb{P} : \left[\omega'\left(E^d\right)\boldsymbol{N}_1 \otimes \boldsymbol{N}_1 + \omega'\left(-E^d\right)\boldsymbol{N}_2 \otimes \boldsymbol{N}_2\right] \\ &= \left[\begin{array}{ccc} \bar{p} + \frac{1}{3}w^a + w^s\cos 2\psi & w^s\sin 2\psi & 0 \\ w^s\sin 2\psi & \bar{p} + \frac{1}{3}w^a - w^s\cos 2\psi & 0 \\ 0 & 0 & \bar{p} - \frac{2}{3}w^a \end{array} \right]_X \end{aligned} \tag{81}$$

with $\bar{p} = Jp = \mathcal{U}'(\ln J)$, where p is the pressure, $w^a := \frac{1}{2}\left(\omega'\left(E^d\right) + \omega'\left(-E^d\right)\right)$ and $w^s := \frac{1}{2}\left(\omega'\left(E^d\right) - \omega'\left(-E^d\right)\right)$ corresponds to the anti-symmetric and symmetric contributions from the stored energy. Note that if the anti-symmetric contribution vanishes, $\omega'\left(E^d\right) = -\omega'\left(-E^d\right)$, the plane stress condition also holds for isochoric deformations as in the infinitesimal linear case. In the spatial configuration, for this isotropic case we can write $\boldsymbol{\sigma} = J^{-1}\boldsymbol{R}\boldsymbol{T}\boldsymbol{R}^T$, which after some algebra yields

$$\boldsymbol{\sigma} = \frac{1}{J} \left[\begin{array}{ccc} \bar{p} + \frac{1}{3}w^a - w^s\cos 2\psi & w^s\sin 2\psi & 0 \\ w^s\sin 2\psi & \bar{p} + \frac{1}{3}w^a + w^s\cos 2\psi & 0 \\ 0 & 0 & \bar{p} - \frac{2}{3}w^a \end{array} \right]_X \tag{82}$$

The sign of the Poynting effect depends on those of w^a and w^s. Note that for $\gamma \geq 0$ we have $\cos 2\psi \in [0, 1)$, so the term $-w^s\cos 2\psi$ vanishes for small γ, but approaches $-w^s$ for large strains. Furthermore, note that for $\bar{p} = 0$, $J = 1$, $2\psi = \pi/2$, the Poynting effect of the linear case is recovered. The simple-shear test under plane strain conditions is obtained setting $\bar{p} = 0$ and $J = 1$. The simple-shear test under plane stress conditions is obtained setting $\bar{p} = \frac{2}{3}w^a$, so

$$\boldsymbol{\sigma} = \frac{1}{J} \left[\begin{array}{ccc} w^a - w^s\cos 2\psi & w^s\sin 2\psi & 0 \\ w^s\sin 2\psi & w^a + w^s\cos 2\psi & 0 \\ 0 & 0 & 0 \end{array} \right]_X \tag{83}$$

A.3. Anisotropic materials

A.3.1. Infinitesimal and pure shear cases

Assuming incompressibility and plane strain deformation ($\varepsilon_3 = 0$), we have in principal strain directions

$$\boldsymbol{\varepsilon} = \begin{bmatrix} \sqrt{\varepsilon_{11}^2 + \varepsilon_{12}^2} & 0 & 0 \\ 0 & -\sqrt{\varepsilon_{11}^2 + \varepsilon_{12}^2} & 0 \\ 0 & 0 & 0 \end{bmatrix}_N = \begin{bmatrix} \gamma/2 & 0 & 0 \\ 0 & -\gamma/2 & 0 \\ 0 & 0 & 0 \end{bmatrix}_N \tag{84}$$

The pure shear strain (by Mohr's circle) is at 45^o, e.g. $\gamma_{45} = 2\varepsilon_{45} = \gamma$. If the principal material direction $\boldsymbol{a}_3$ is perpendicular to the shearing plane, we can obtain the deviatoric stresses in a quite straightforward manner —just consider the relevant 3×3 box and note that $\mu_{11}^* (\varepsilon_1)$ and $\mu_{22}^* (\varepsilon_2)$ are the same function, but the actual value is different because they are evaluated at different strains

$$\begin{bmatrix} \frac{8}{9}\mu_{11}^* + \frac{2}{9}\mu_{22}^* + \frac{2}{9}\mu_{33}^* & \frac{2}{9}\mu_{33}^* - \frac{4}{9}\mu_{22}^* - \frac{4}{9}\mu_{11}^* & \frac{2}{9}\mu_{22}^* - \frac{4}{9}\mu_{11}^* - \frac{4}{9}\mu_{33}^* \\ \frac{2}{9}\mu_{33}^* - \frac{4}{9}\mu_{22}^* - \frac{4}{9}\mu_{11}^* & \frac{2}{9}\mu_{11}^* + \frac{8}{9}\mu_{22}^* + \frac{2}{9}\mu_{33}^* & \frac{2}{9}\mu_{11}^* - \frac{4}{9}\mu_{22}^* - \frac{4}{9}\mu_{33}^* \\ \frac{2}{9}\mu_{22}^* - \frac{4}{9}\mu_{11}^* - \frac{4}{9}\mu_{33}^* & \frac{2}{9}\mu_{11}^* - \frac{4}{9}\mu_{22}^* - \frac{4}{9}\mu_{33}^* & \frac{2}{9}\mu_{11}^* + \frac{2}{9}\mu_{22}^* + \frac{8}{9}\mu_{33}^* \end{bmatrix} \begin{Bmatrix} \gamma/2 \\ -\gamma/2 \\ 0 \end{Bmatrix}$$
$$= \begin{Bmatrix} \frac{1}{3}\gamma\left(2\mu_{11}^* + \mu_{22}^*\right) \\ -\frac{1}{3}\gamma\left(\mu_{11}^* + 2\mu_{22}^*\right) \\ -\frac{1}{3}\gamma\left(\mu_{11}^* - \mu_{22}^*\right) \end{Bmatrix} \equiv \begin{Bmatrix} \frac{1}{3}\gamma\left(2\mu_{11}^t + \mu_{11}^c\right) \\ -\frac{1}{3}\gamma\left(\mu_{11}^t + 2\mu_{11}^c\right) \\ -\frac{1}{3}\gamma\left(\mu_{11}^t - \mu_{11}^c\right) \end{Bmatrix} \tag{85}$$

which have no shear stress in that system of representation. However, there is a shear stress in other systems. At 45^o

$$\boldsymbol{\sigma} = \begin{bmatrix} \frac{1}{3}\mu_{11}^a\gamma & \mu_{11}^s\gamma & 0 \\ \mu_{11}^s\gamma & \frac{1}{3}\mu_{11}^a\gamma & 0 \\ 0 & 0 & -\frac{2}{3}\mu_{11}^a\gamma \end{bmatrix}_X \tag{86}$$

where

$$\mu_{11}^s = \tfrac{1}{2}\left(\mu_{11}^t + \mu_{11}^c\right) \quad \text{and} \quad \mu_{11}^a = \tfrac{1}{2}\left(\mu_{11}^t - \mu_{11}^c\right)$$

i.e. $\tau_{45} = \mu_{11}^s\gamma$, the shear modulus is $G_{45} = \mu_{11}^s$ and the Poynting effect is given by $\frac{1}{3}\mu_{11}^a\gamma$. Obviously if $\mu_{11}^t = \mu_{11}^c \equiv \mu_{11}$ we recover $G_{45} = \mu_{11}$.

It is straightforward to verify that in the large strain case we have —we make here use of the co-linearity of stresses and strains and of the isochoric condition

$$\boldsymbol{\sigma} = \boldsymbol{T} = \begin{bmatrix} \frac{1}{3}w_{11}^a(E) & w_{11}^s(E) & \\ w_{11}^s(E) & \frac{1}{3}w_{11}^a(E) & \\ & & -\frac{2}{3}w_{11}^a(E) \end{bmatrix}_X \tag{87}$$

again with equivalent definitions for E, w^a, w^s as in the isotropic case.

If the pure-shear plane contains the preferred direction in an aligned manner, say the third direction working in tension, then we have for example for the infinitesimal case

$$\begin{bmatrix} \frac{8}{9}\mu_{11}^* + \frac{2}{9}\mu_{22}^* + \frac{2}{9}\mu_{33}^* & \frac{2}{9}\mu_{33}^* - \frac{4}{9}\mu_{22}^* - \frac{4}{9}\mu_{11}^* & \frac{2}{9}\mu_{22}^* - \frac{4}{9}\mu_{11}^* - \frac{4}{9}\mu_{33}^* \\ \frac{2}{9}\mu_{33}^* - \frac{4}{9}\mu_{22}^* - \frac{4}{9}\mu_{11}^* & \frac{2}{9}\mu_{11}^* + \frac{8}{9}\mu_{22}^* + \frac{2}{9}\mu_{33}^* & \frac{2}{9}\mu_{11}^* - \frac{4}{9}\mu_{22}^* - \frac{4}{9}\mu_{33}^* \\ \frac{2}{9}\mu_{22}^* - \frac{4}{9}\mu_{11}^* - \frac{4}{9}\mu_{33}^* & \frac{2}{9}\mu_{11}^* - \frac{4}{9}\mu_{22}^* - \frac{4}{9}\mu_{33}^* & \frac{2}{9}\mu_{11}^* + \frac{2}{9}\mu_{22}^* + \frac{8}{9}\mu_{33}^* \end{bmatrix} \begin{Bmatrix} -\gamma/2 \\ 0 \\ \gamma/2 \end{Bmatrix}$$
$$= \begin{Bmatrix} -\frac{1}{3}\gamma\left(2\mu_{11}^c + \mu_{33}^t\right) \\ \frac{1}{3}\gamma\left(\mu_{11}^c - \mu_{33}^t\right) \\ \frac{1}{3}\gamma\left(\mu_{11}^c + 2\mu_{33}^t\right) \end{Bmatrix} = \begin{Bmatrix} -\mu_{11}^c\gamma - \frac{2}{3}\bar{\mu}_{33}^t\gamma \\ -\frac{2}{3}\bar{\mu}_{33}^t\gamma \\ \mu_{11}^c\gamma + \frac{4}{3}\bar{\mu}_{33}^t\gamma \end{Bmatrix} \tag{88}$$

with the definition $\bar{\mu}_{33}^t := \frac{1}{2}\left(\mu_{33}^t - \mu_{11}^c\right)$ (which can be thought as half the net contribution of the fiber over that of the matrix if the latter has the same behavior in tension and compression). Then,

$$[\boldsymbol{\sigma}]_N = \begin{bmatrix} -\mu_{11}^c\gamma - \frac{2}{3}\bar{\mu}_{33}^t\gamma & & \\ & -\frac{2}{3}\bar{\mu}_{33}^t\gamma & \\ & & \mu_{11}^c\gamma + \frac{4}{3}\bar{\mu}_{33}^t\gamma \end{bmatrix} \tag{89}$$

and

$$[\boldsymbol{\sigma}]_X = \begin{bmatrix} \frac{1}{3}\bar{\mu}_{33}^t\gamma & 0 & \mu_{11}^c\gamma + \bar{\mu}_{33}^t\gamma \\ 0 & -\frac{2}{3}\bar{\mu}_{33}^t\gamma & 0 \\ \mu_{11}^c\gamma + \bar{\mu}_{33}^t\gamma & 0 & \frac{1}{3}\bar{\mu}_{33}^t\gamma \end{bmatrix} \tag{90}$$

which can be compared to Eq. (69). In this case the equivalent shear stiffness is $G_{13} = \frac{1}{2}\left(\mu_{11}^c + \mu_{33}^t\right)$, and the Poynting effect is given by $\bar{\mu}_{33}^t = \frac{1}{2}\left(\mu_{33}^t - \mu_{11}^c\right)$. Note that a tension-compression switch for fibers may be immediately implemented just taking $\mu_{33}^c = \mu_{11}^c$. In such a case, if fibers work in compression a similar equation to Eq. (86) is recovered.

For large strains, $E_{ij} = 0$ for $i \neq j$ in this test with the fibers aligned, so the generalized Kirchhoff stress tensor is coincident with the rotated Kirchhoff stress tensor and

$$\boldsymbol{T} = \bar{p}\boldsymbol{I} + \omega_{11}\left(-E^d\right)\boldsymbol{M}_1^d + \omega_{33}\left(E^d\right)\boldsymbol{L}_{33}^d \tag{91}$$

with $E^d = \ln\lambda$. In this system of representation X, it is easy to show that a similar

equation to Eq. (90) is obtained

$$\begin{cases} T_{11} = J\sigma_{11} = Jp + \frac{1}{6}\left[\omega'_{33}\left(E\right) + \omega'_{11}\left(-E\right)\right] \\ T_{22} = J\sigma_{22} = Jp - \frac{1}{3}\left[\omega'_{33}\left(E\right) + \omega'_{11}\left(-E\right)\right] \\ T_{33} = J\sigma_{33} = Jp + \frac{1}{6}\left[\omega'_{33}\left(E\right) + \omega'_{11}\left(-E\right)\right] \\ T_{13} = J\sigma_{13} = \frac{1}{2}\left[\omega'_{33}\left(E\right) - \omega'_{11}\left(-E\right)\right] \\ T_{12} = T_{23} = 0 \end{cases} \tag{92}$$

Noteworthy, the Poynting effect may be modified by the consideration of an isotropic contribution with different behavior in tension and compression, see Eqs. (50) and (75).

A.3.2. Simple shear case

Recalling the eigenvalue $E^d = \ln \lambda^d = \ln\left(1/\tan\psi\right) = -\ln\left(\tan\psi\right)$, the invariants are

$$\begin{aligned} E^d_{ij}\left(\psi\left(\gamma\right)\right) &= \boldsymbol{E} : \boldsymbol{L}^d_{ij} = \left(E^d \boldsymbol{M}_1 - E^d \boldsymbol{M}_2\right) : \boldsymbol{L}^d_{ij} \\ &= E^d\left(\psi\left(\gamma\right)\right)\left(\boldsymbol{M}_1\left(\psi\left(\gamma\right)\right) : \boldsymbol{L}^d_{ij}\right) - E^d\left(\psi\left(\gamma\right)\right)\left(\boldsymbol{M}_2\left(\psi\left(\gamma\right)\right) : \boldsymbol{L}^d_{ij}\right) \end{aligned} \tag{93}$$

where $\psi\left(\gamma\right) = \left(1/2\right)\arctan\left(2/\gamma\right) \in \left[\pi/4, 0\right)$ and $\boldsymbol{M}_i\left(\psi\right)$ is given above. Then

$$\boldsymbol{T} = \mathcal{U}'\left(\ln J\right)\boldsymbol{I} + \sum_{i,j} \omega'_{ij}\left(E^d_{ij}\left(\psi\left(\gamma\right)\right)\right)\boldsymbol{L}^d_{ij} \tag{94}$$

in which symmetries must be taken into account. Since this case is mathematically elaborate, a numerical solution is advisable in general. However, we can particularize the problem to a transverse isotropic material with fibers perpendicular to the shearing direction, i.e. $\boldsymbol{a}_3 = \left[1,0,0\right]^T_X$. Then we have

$$\boldsymbol{L}_{33} = \boldsymbol{a}_3 \otimes \boldsymbol{a}_3 = \begin{bmatrix} 1 & 0 & 0 \\ 0 & 0 & 0 \\ 0 & 0 & 0 \end{bmatrix}_X \quad \text{and} \quad \boldsymbol{L}^d_{33} = \begin{bmatrix} \frac{2}{3} & 0 & 0 \\ 0 & -\frac{1}{3} & 0 \\ 0 & 0 & -\frac{1}{3} \end{bmatrix}_X \tag{95}$$

Working in logarithmic strains, since there is no out-of-plane shear strain, $E_{12} = 0$, and choosing $\boldsymbol{a}_1 = \left[0,0,1\right]^T_X$ and $\boldsymbol{a}_2 = \left[0,1,0\right]^T_X$,

$$\boldsymbol{L}^d_{11} = \begin{bmatrix} -\frac{1}{3} & 0 & 0 \\ 0 & -\frac{1}{3} & 0 \\ 0 & 0 & \frac{2}{3} \end{bmatrix}_X \text{ and } \boldsymbol{L}^d_{22} = \begin{bmatrix} -\frac{1}{3} & 0 & 0 \\ 0 & \frac{2}{3} & 0 \\ 0 & 0 & -\frac{1}{3} \end{bmatrix}_X \tag{96}$$

$$\boldsymbol{L}^d_{13} \equiv \boldsymbol{L}_{13} = \begin{bmatrix} 0 & 0 & \frac{1}{2} \\ 0 & 0 & 0 \\ \frac{1}{2} & 0 & 0 \end{bmatrix}_X \; ; \; \boldsymbol{L}_{23} \equiv \boldsymbol{L}^d_{23} = \begin{bmatrix} 0 & \frac{1}{2} & 0 \\ \frac{1}{2} & 0 & 0 \\ 0 & 0 & 0 \end{bmatrix}_X$$

Then, in the plane with $E_{12} = 0$

$$E^d_{33} = \boldsymbol{E} : \boldsymbol{L}^d_{33} = E^d \cos(2\psi) \tag{97}$$

$$E^d_1 = \boldsymbol{E} : \boldsymbol{L}^d_{11} = 0 \;\; \text{and} \;\; E^d_2 = -E^d \cos(2\psi) \tag{98}$$

$$\left(E^{\#}_{13}\right)^2 = \left(E^d \sin(2\psi)\right)^2 \tag{99}$$

In order to make the exposition simple and concrete, consider a bi-linear model in terms of logarithmic deviatoric strains. Then

$$\boldsymbol{T} = \bar{p}\boldsymbol{I} + \sum_{i,j} 2\mu^*_{ij} E^d_{ij} \boldsymbol{L}^d_{ij} \tag{100}$$

$$= \bar{p}\boldsymbol{I} - 2\mu^c_{11} E^d \cos(2\psi)\, \boldsymbol{L}^d_{22} + 2\mu^t_{33} E^d \cos(2\psi)\, \boldsymbol{L}^d_{33} + 2\mu_{13} E^d \sin(2\psi)\, \boldsymbol{L}_{23} \tag{101}$$

i.e., in the system of representation X

$$\begin{cases} T_{11} = \bar{p} + \frac{2}{3}\left(\mu^c_{11} + 2\mu^t_{33}\right) E^d \cos(2\psi) \\ T_{22} = \bar{p} + \frac{2}{3}\left(-2\mu^c_{11} - \mu^t_{33}\right) E^d \cos(2\psi) \\ T_{12} = \mu_{13} E^d \sin(2\psi) \\ T_{33} = \bar{p} + \frac{2}{3}\left(\mu^c_{11} - \mu^t_{33}\right) E^d \cos(2\psi) \end{cases} \tag{102}$$

Since in this case the principal strain directions change during the deformation, the transformation to Cauchy stresses in analytical form is involved. To obtain the Cauchy stresses, we first compute the rotated Kirchhoff stress $\bar{\boldsymbol{\tau}}$ which has the same diagonal terms as $\boldsymbol{T}$, but with the shear terms [38]

$$\bar{\tau}_{ij} = \frac{2\lambda_j \lambda_i \left(\ln \lambda_j - \ln \lambda_i\right)}{\lambda^2_j - \lambda^2_i} T_{ij}, \;\; i \neq j \tag{103}$$

The Cauchy stress is then obtained as $\boldsymbol{\sigma} = J^{-1}\boldsymbol{R}\bar{\boldsymbol{\tau}}\boldsymbol{R}^T$, where $\boldsymbol{R}$ is given in Eq. (77). It can be seen that the effective shear stiffness depends not only on μ_{13}, but also on μ^c_{11}, μ^t_{33} as in previous cases. However μ_{13} does not affect the Poynting effect, which as in the previous cases depends on the axial terms μ^*_{11} and μ^*_{33}.

A.4. Twisting of a cuboid

We now address the twisting of a unit-length cuboid using the four transversely isotropic material models discussed in this paper. A fully integrated single Brick finite element with mixed formulation u/p 8/1 $Q1/P0$ is employed [43]. In Figure 15, the undeformed and deformed elements along with the displacement loads being applied at nodes (vertices) are shown. The anisotropic (fiber) direction is oriented along the twisting axis, i.e. axis Y in Figure 15. The axial displacements at the loading faces are constrained by means of $u_y = 0$ at nodes. The "radial" displacement of every node is left free and a "circumferential" displacement of $u = \sqrt{2}/4\,\mathrm{mm}$ is prescribed at each node as indicated in the figure. The final deformed mesh is then determined by the nearly-incompressible response, which is imposed through a volumetric penalty approach (we use a volumetric strain energy $\mathcal{U}(J) = \frac{1}{2}\kappa(J-1)^2$ with $\kappa = 10^3\,\mathrm{MPa}$), becoming the same deformed mesh for the four simulations performed. The reaction forces predicted at nodes by each model are different though, as we see next.

This finite element model simulates, qualitatively, the twisting of a ligament. Since the fiber direction is oriented along the twisting axis, the shear mode undergone by the material corresponds to the so-called perpendicular shear, see Figure 1*c* in Ref. [59]. As a result of the different material stiffness in the isotropic plane and the anisotropic direction, the material tends to contract along the twisting axis. Since we are constraining the displacements along that axis, traction (positive) reaction forces should be exerted at the loading faces of the cuboid such that $u_y = 0$ at nodes as a result. By convention, this traction force, that prevents the contraction of the cuboid in the axial direction, represents a *negative* Poynting effect [59].

The nodal forces predicted by each model are given in Table 1. The results given by the analytical models of Sections 4.1 and 4.2 are to be compared to the results given by their homologous WYPiWYG models of Sections 5.1 and 5.2, respectively. We can observe that the predictions given by the analytical models and their respective WYPiWYG models for the twisting (shear-like) force exerted at nodes in the direction of the displacements are in very good agreement to each other. On other side, both Reinforcing and Humphrey–Yin models predict a positive traction force along the Y-axis, i.e. a negative Poynting effect, as expected. We can also observe that their respective WYPiWYG models also predict negative Poynting effects, even though the traction reaction forces are lower in both cases. Similarly to what is explained in Section 6 for the case $\alpha = 60\,^\circ$, these differences can be attributed to the different couplings between strain components that the models present in generic out-of-axes deformations. However, as also discussed in that Section regarding, for example, the strain localization of the Standard Reinforcing model, we can see that our WYPiWYG models are again capable of reproducing the main characteristics

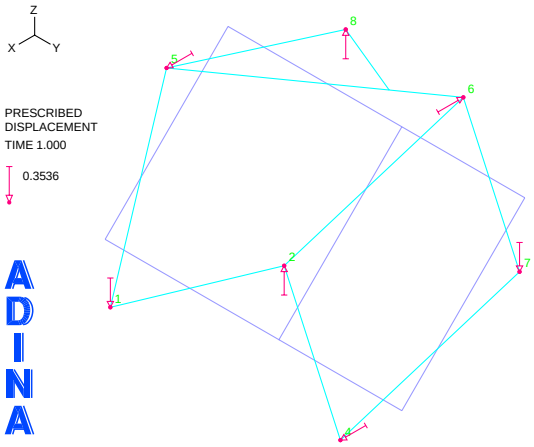

Figure 15: Twist of a 1 mm-length cuboid with constrained axial displacements at the loading faces, i.e. $u_y = 0$ at nodes (vertices). The "radial" displacement of every node is free and a "circumferential" displacement of $u = \sqrt{2}/4$ mm is prescribed at each node as indicated in the figure.

of both analytical models in this specific loading case, i.e. the same sign and order of magnitude of the Poynting effect. The reader should not forget that our models have been characterized with two tension-compression uniaxial tests and an additional response curve from a pure shear test (which are exactly reproduced), while this twisting cuboid example resembles, to some extent, a simple shear test.

Finally, we want also to remark that the finite element model used in this example, consisting of a single $Q1/P0$ element, has been chosen in order to perform a simple

Table 1: Nodal force reactions (in MPa) at maximum load predicted by the four different models addressed in this example. Twist Force refers to the (shear-like) reaction force at each node along the corresponding applied displacement direction. Axial Force refers to the (normal-like) traction force at each node in the Y-axis direction, i.e. a negative Pointing effect .

Model	Twist Force	Axial Force
Reinforcing	3.830E−03	8.499E−03
WYPiWYG (Reinforcing)	4.543E−03	1.971E−03
Humphrey–Yin	5.549E−03	1.101E−02
WYPiWYG (Humphrey–Yin)	5.931E−03	2.511E−03

comparison of the predictions given by the models during the (ideal) twisting of a cuboid. However, if a realistic simulation of the twisting of a ligament is to be performed, for either material characterization from experimental data or further prediction of results, a more appropriate finite element model should be employed. As we show in Ref. [51], even a single $Q2/P1$ element would be able to reproduce very accurately the actual response of a cuboid under simple shear.

References

[1] Humphrey, J. D. (2013). Cardiovascular solid mechanics: cells, tissues, and organs. Springer, New York.

[2] Fung, Y. C. (2013). Biomechanics: mechanical properties of living tissues. Springer, New York.

[3] Shariff, M. H. B. M. (2008). Nonlinear transversely isotropic elastic solids: an alternative representation. The Quarterly Journal of Mechanics & Applied Mathematics, 61(2), 129-149.

[4] Shariff, M. H. B. M. (2011). Physical invariants for nonlinear orthotropic solids. International Journal of Solids and Structures, 48(13), 1906-1914.

[5] Criscione, J. C., Douglas, A. S., & Hunter, W. C. (2001). Physically based strain invariant set for materials exhibiting transversely isotropic behavior. Journal of the Mechanics and Physics of Solids, 49(4), 871-897.

[6] Criscione, J. C., Humphrey, J. D., Douglas, A. S., & Hunter, W. C. (2000). An invariant basis for natural strain which yields orthogonal stress response terms in isotropic hyperelasticity. Journal of the Mechanics and Physics of Solids, 48(12), 2445-2465.

[7] Holzapfel, G. A. (2002). Nonlinear Solid Mechanics: A Continuum Approach for Engineering. Wiley, Chichester.

[8] Criscione, J. (2005). Rivlin's representation formula is ill-conceived for the determination of response functions via biaxial testing. In: The Rational Spirit in Modern Continuum Mechanics, CS Man, RL Fosdick (eds), Kuwler, 197-215.

[9] Murphy, J. G. (2013). Transversely isotropic biological, soft tissue must be modelled using both anisotropic invariants. European Journal of Mechanics-A/Solids, 42, 90-96.

[10] Murphy, J. G. (2014). Evolution of anisotropy in soft tissue. Proceedings of the Royal Society A; 470(2161), 20130548

[11] Destrade, M., Mac Donald, B., Murphy, J.G., Saccomandi, G. (2013). At least three invariants are necessary to model the mechanical response of incompressible, transversely isotropic materials. Computational Mechanics, 52(4), 959-969.

[12] Horgan, C. O., Murphy, J. G. (2014). Some unexpected behaviour in shear for elasticity models of arterial tissue that only use the I1, I4, I6 invariants. IMA Journal of Applied Mathematics, 79, 820-829.

[13] Murphy, J. G., Biwa, S. (2017). The counterintuitive mechanical response in simple tension of arterial models that are separable functions of the I1, I4, I6 invariants. International Journal of Non-Linear Mechanics, 90, 72-81.

[14] Feng, Y., Qiu, S., Xia, X., Ji, S., Lee, C. H. (2017). A computational study of invariant I_5 in a nearly incompressible transversely isotropic model for white matter. Journal of Biomechanics, 57, 146-151.

[15] Feng, Y., Okamoto, R. J., Genin, G. M., Bayly, P. V. (2016). On the accuracy and fitting of transversely isotropic material models. Journal of the Mechanical Behavior of Biomedical Materials, 61, 554-566.

[16] Melnik, A. V., Da Rocha, H. B., Goriely, A. (2015). On the modeling of fibre dispersion in fibre-reinforced elastic materials. International Journal of Non-Linear Mechanics, 75, 92-106.

[17] Latorre, M., Romero, X., Montáns, F. J. (2016). The relevance of transverse deformation effects in modeling soft biological tissues. International Journal of Solids and Structures, 99, 57-70.

[18] Shariff, M. H. B. M., Bustamante, R., Merodio, J. (2017). Rate type constitutive equations for fiber reinforced nonlinearly vicoelastic solids using spectral invariants. Mechanics Research Communications, 99, 60-64.

[19] Shariff, M. H. B. M., Bustamante, R., Merodio, J. (2017). On the spectral analysis of residual stress in finite elasticity. IMA Journal of Applied Mathematics, 82(3), 656-680.

[20] Baek, S., Gleason, R. L., Rajagopal, K. R., Humphrey, J. D. (2007). Theory of small on large: potential utility in computations of fluid–solid interactions in arteries. Computer Methods in Applied Mechanics and Engineering, 196(31), 3070-3078.

[21] Jor, J. W., Nash, M. P., Nielsen, P. M., Hunter, P. J. (2011). Estimating material parameters of a structurally based constitutive relation for skin mechanics. Biomechanics and modeling in mechanobiology, 10(5), 767-778.

[22] Sussman, T., Bathe, K.J. A model of incompressible isotropic hyperelastic material behavior using spline interpolations of tension-compression test data. Communications in Numerical Methods in Engineering, 25(1), 53–63, 2009.

[23] Shariff, M. H. B. M. (1999). Physical parameters strain energy function for rubberlike materials. In: Constitutive Models for Rubber, A Dorfmann, A Muhr (Eds). Balkema, Rotterdam, 131-137.

[24] Weber, G., & Anand, L. (1990). Finite deformation constitutive equations and a time integration procedure for isotropic, hyperelastic-viscoplastic solids. Computer Methods in Applied Mechanics and Engineering, 79(2), 173-202.

[25] Eterovic, A. L., & Bathe, K. J. (1990). A hyperelastic-based large strain elasto-plastic constitutive formulation with combined isotropic-kinematic hardening using the logarithmic stress and strain measures. International Journal for Numerical Methods in Engineering, 30(6), 1099-1114.

[26] Simo, J. C. (1992). Algorithms for static and dynamic multiplicative plasticity that preserve the classical return mapping schemes of the infinitesimal theory. Computer Methods in Applied Mechanics and Engineering, 99(1), 61-112.

[27] Caminero, M. Á., Montáns, F. J., & Bathe, K. J. (2011). Modeling large strain anisotropic elasto-plasticity with logarithmic strain and stress measures. Computers & Structures, 89(11), 826-843.

[28] Latorre, M., Montáns, F. J. (2013). Extension of the Sussman–Bathe spline-based hyperelastic model to incompressible transversely isotropic materials. Computers & Structures, 122, 13-26.

[29] Latorre, M. Montáns, F.J. What-You-Prescribe-Is-What-You-Get orthotropic hyperelasticity. Computational Mechanics, 53(6), 1279–1298, 2014.

[30] Crespo, J., Latorre, M., Montáns, F. J. (2017). WYPiWYG hyperelasticity for isotropic, compressible materials. Computational Mechanics, 59, 73–92.

[31] Latorre M, Montáns FJ (2017). WYPiWYG hyperelasticity without inversion formula: Application to passive ventricular myocardium. Computers and Structures 185, 47–58.

[32] Shariff, M. H. B. M. (2016). Anisotropic separable free energy functions for elastic and non-elastic solids. Acta Mechanica, 11(227), 3213-3237.

[33] Merodio, J., Ogden, R. W. (2005). Mechanical response of fiber-reinforced incompressible non-linearly elastic solids. International Journal of Non-Linear Mechanics, 40(2), 213-227.

[34] Du, Z., Zhang, Y., Zhang, W., & Guo, X. (2016). A new computational framework for materials with different mechanical responses in tension and compression and its applications. International Journal of Solids and Structures, 100, 54-73.

[35] Du, Z., & Guo, X. (2014). Variational principles and the related bounding theorems for bi-modulus materials. Journal of the Mechanics and Physics of Solids, 73, 183-211.

[36] Bathe K. J. (2014). Finite element procedures. 2nd ed. K. J. Bathe, Watertown.

[37] Latorre, M., & Montáns, F. J. (2014). On the interpretation of the logarithmic strain tensor in an arbitrary system of representation. International Journal of Solids and Structures, 51(7), 1507-1515.

[38] Latorre, M., & Montáns, F. J. (2016). Stress and strain mapping tensors and general work-conjugacy in large strain continuum mechanics. Applied Mathematical Modelling, 40(5), 3938-3950.

[39] Latorre, M., & Montáns, F. J. (2015). Material-symmetries congruency in transversely isotropic and orthotropic hyperelastic materials. European Journal of Mechanics-A/Solids, 53, 99-106.

[40] Treloar, L. R. G. (1975). The Physics of Rubber Elasticity. Oxford University Press, Oxford.

[41] Pancheri, F. Q., & Dorfmann, L. (2014). Strain-controlled biaxial tension of natural rubber: new experimental data. Rubber Chemistry and Technology, 87(1), 120-138.

[42] Jones, R.M. (1999). Mechanics of Composite Materials, 2nd ed. Taylor & Francis, Philadelphia.

[43] Bathe K. J. (2014). Finite element procedures. 2nd ed. K. J. Bathe, Watertown.

[44] Borja, R. I., Lin, C. H., & Montáns, F. J. (2001). Cam-Clay plasticity, Part IV: Implicit integration of anisotropic bounding surface model with nonlinear hyperelasticity and ellipsoidal loading function. Computer methods in applied mechanics and engineering, 190(26), 3293-3323.

[45] Latorre, M., De Rosa, E., & Montáns, F. J. (2017). Understanding the need of the compression branch to characterize hyperelastic materials. International Journal of Non-Linear Mechanics, 89, 14-24.

[46] Ogden, R. W., Saccomandi, G., Sgura, I. (2004). Fitting hyperelastic models to experimental data. Computational Mechanics, 34(6), 484-502.

[47] Destrade, M., Gilchrist, M. D., Prikazchikov, D. A., Saccomandi, G. (2008). Surface instability of sheared soft tissues. Journal of biomechanical engineering, 130(6), 061007.

[48] Ning, X., Zhu, Q., Lanir, Y., Margulies, S. S. (2006). A transversely isotropic viscoelastic constitutive equation for brainstem undergoing finite deformation. Journal of biomechanical engineering, 128(6), 925-933.

[49] Morrow, D. A., Donahue, T. L. H., Odegard, G. M., Kaufman, K. R. (2010). Transversely isotropic tensile material properties of skeletal muscle tissue. Journal of the mechanical behavior of biomedical materials, 3(1), 124-129.

[50] Humphrey, J. D., Yin, F. C. (1987). A new constitutive formulation for characterizing the mechanical behavior of soft tissues. Biophysical journal, 52(4), 563.

[51] Latorre, M., Peña, E., Montáns, F. J. (2016). Determination and Finite Element Validation of the WYPiWYG Strain Energy of Superficial Fascia from Experimental Data. Annals of Biomedical Engineering, doi: 10.1007/s10439-016-1723-2.

[52] Romero, X., Latorre, M., & Montáns, F. J. (2017). Determination of the WYPiWYG strain energy density of skin through finite element analysis of the experiments on circular specimens. Finite Elements in Analysis and Design, 134, 1-15.

[53] ADINA, Theory and Modelling Guide (2012). ARD 12-8. ADINA R&D. Watertown.

[54] Moerman, K. M., Simms, C. K., Nagel, T. (2016). Control of tension–compression asymmetry in Ogden hyperelasticity with application to soft tissue modelling. Journal of the Mechanical Behavior of Biomedical Materials, 56, 218-228.

[55] Skacel, P, Bursa, J (2016). Poisson's ratio of arterial wall–Inconsistency of constitutive models with experimental data. Journal of the Mechanical Behavior of Biomedical Materials, 54, 316-327.

[56] Loret, B., Rizzi, E. (1997). Anisotropic stiffness degradation triggers onset of strain localization. International Journal of Plasticity, 13(5), 447-459.

[57] Chadwick P (1999). Continuum Mechanics. Concise Theory and Problems. Dover, Mineola.

[58] Horgan, C. O., & Murphy, J. G. (2017). Poynting and reverse Poynting effects in soft materials. Soft Matter, in press. Doi: 10.1039/C7SM00992E

[59] Destrade, M., Horgan, C. O., Murphy, J. G. (2015). Dominant negative Poynting effect in simple shearing of soft tissues. Journal of Engineering Mathematics, 95(1), 87-98.

[60] Horgan, C. O., & Murphy, J. G. (2015). Reverse Poynting effects in the torsion of soft biomaterials. Journal of Elasticity, 118(2), 127-140.

[61] Horgan, C. O., & Murphy, J. G. (2012). On the modeling of extension-torsion experimental data for transversely isotropic biological soft tissues. Journal of Elasticity, 108(2), 179-191.

[62] Mihai, L. A., & Goriely, A. (2011). Positive or negative Poynting effect? The role of adscititious inequalities in hyperelastic materials. In Proc. R. Soc. A (Vol. 467, No. 2136, pp. 3633-3646).

[63] Goriely, A., & Tabor, M. (2013). Rotation, inversion and perversion in anisotropic elastic cylindrical tubes and membranes. In Proc. R. Soc. A (Vol. 469, No. 2153, p. 20130011). The Royal Society.